



## RESEARCH ARTICLE

# Molecular mechanisms of *Streptococcus pneumoniae*-targeted autophagy via pneumolysin, Golgi-resident Rab41, and Nedd4-1-mediated K63-linked ubiquitination

Michinaga Ogawa<sup>1</sup>  | Ryuta Matsuda<sup>1,2</sup> | Naoki Takada<sup>1,3</sup> | Mikado Tomokiyo<sup>1,4</sup> | Shouji Yamamoto<sup>1</sup> | Sayaka Shizukushi<sup>1,5</sup> | Toshiyuki Yamaji<sup>6</sup> | Yuko Yoshikawa<sup>7</sup> | Mitsutaka Yoshida<sup>8</sup> | Isei Tanida<sup>9</sup> | Masato Koike<sup>9</sup> | Miyo Murai<sup>2</sup> | Hidetoshi Morita<sup>10</sup> | Haruko Takeyama<sup>3</sup> | Akihide Ryo<sup>5</sup> | Jun-Lin Guan<sup>11</sup> | Masahiro Yamamoto<sup>12</sup> | Jun-ichiro Inoue<sup>13</sup> | Toru Yanagawa<sup>14</sup> | Mitsunori Fukuda<sup>15</sup>  | Hiroshi Kawabe<sup>16</sup> | Makoto Ohnishi<sup>1</sup>

<sup>1</sup>Department of Bacteriology I, National Institute of Infectious Diseases, Tokyo, Japan

<sup>2</sup>Department of Health Sciences, Saitama Prefectural University, Saitama, Japan

<sup>3</sup>Department of Life Science and Medical Bioscience, Waseda University, Tokyo, Japan

<sup>4</sup>School of Veterinary Medicine, Azabu University, Sagami-hara-shi, Kanagawa, Japan

<sup>5</sup>Department of Microbiology, Yokohama City University Graduate School of Medicine, Yokohama-shi, Kanagawa, Japan

<sup>6</sup>Department of Biochemistry and Cell Biology, National Institute of Infectious Diseases, Tokyo, Japan

<sup>7</sup>Division of Veterinary Hygiene and Public Health, Department of Preventive Veterinary Medicine, School of Veterinary Medicine, Faculty of Veterinary Science, Nippon Veterinary and Life Science University, Tokyo, Japan

<sup>8</sup>Division of Ultrastructural Research, BioMedical Research Center, Juntendo University, Tokyo, Japan

<sup>9</sup>Department of Cell Biology and Neuroscience, Graduate School of Medicine, Juntendo University, Tokyo, Japan

<sup>10</sup>Laboratory of Animal Applied Microbiology, Graduate School of Environmental and Life Science, Okayama University, Okayama, Japan

<sup>11</sup>Division of Molecular Medicine and Genetics, Department of Internal Medicine, University of Michigan Medical School, Ann Arbor, Michigan, USA

<sup>12</sup>Department of Immunoparasitology, Research Institute for Microbial Diseases, Osaka University, Osaka, Japan

<sup>13</sup>Division of Cellular and Molecular Biology, Department of Cancer Biology, The Institute of Medical Science, The University of Tokyo, Tokyo, Japan

<sup>14</sup>Faculty of Medicine, University of Tsukuba, Ibaraki, Japan

<sup>15</sup>Laboratory of Membrane Trafficking Mechanisms, Department of Developmental Biology and Neurosciences, Graduate School of Life Sciences, Tohoku University, Sendai, Miyagi, Japan

<sup>16</sup>Department of Molecular Neurobiology, Max Planck Institute of Experimental Medicine, Göttingen, Germany

## Correspondence

Michinaga Ogawa, Department of Bacteriology I, National Institute of Infectious Diseases, 1-23-1, Toyama, Shinjuku-ku, Tokyo 162-8640, Japan.

Email: micogawa@nih.go.jp

## Funding information

Uehara Memorial Foundation; Naito Foundation; Ministry of Education, Culture, Sports, Science, and Technology (MEXT), Grant/Award Numbers: 25460555, 16K08800, 17H05682 and 16H01189

## Abstract

*Streptococcus pneumoniae* is the most common causative agent of community-acquired pneumonia and can penetrate epithelial barriers to enter the bloodstream and brain. We investigated intracellular fates of *S. pneumoniae* and found that the pathogen is entrapped by selective autophagy in pneumolysin- and ubiquitin-p62-LC3 cargo-dependent manners. Importantly, following induction of autophagy, Rab41 was relocated from the Golgi apparatus to *S. pneumoniae*-containing autophagic vesicles (PcAV), which were only formed in the presence of Rab41-positive intact Golgi apparatuses. Moreover, subsequent localization and regulation of K48- and K63-linked polyubiquitin chains in and on PcAV were clearly distinguishable from each other. Finally, we found that E3 ligase Nedd4-1 was recruited to PcAV and played a pivotal role in K63-linked polyubiquitin chain (K63Ub) generation on PcAV,

promotion of PcAV formation, and elimination of intracellular *S. pneumoniae*. These findings suggest that Nedd4-1-mediated K63Ub deposition on PcAV acts as a scaffold for PcAV biogenesis and efficient elimination of host cell-invaded pneumococci.

#### KEYWORDS

K48- and K63-linked polyUb chain, Nedd4-1, pneumolysin, Rab41 (Rab43), selective autophagy, *Streptococcus pneumoniae*

## 1 | INTRODUCTION

*Streptococcus pneumoniae* (*S. pneumoniae*) is a major encapsulated Gram-positive pathogen, colonising the human nasopharynx (Kadioglu, Weiser, Paton, & Andrew, 2008). Depending on host susceptibility, *S. pneumoniae* causes sinusitis, acute otitis media, and pneumonia. In infants of <5 years of age and immunocompromised elderly people, *S. pneumoniae* can cause invasive pneumococcal disease (IPD), which is associated with high incidence of morbidity and mortality and sepsis and meningitis (Nakano et al., 2016). During severe infections, *S. pneumoniae* colonising at nasopharyngeal epithelial tissues invades and cross these to enter the bloodstream and brain via the blood-brain barrier. Both innate and adaptive immune processes control the colonising bacteria, and nasopharyngeal and lung epithelia are the first line of defence against pneumococcal infections. Although widespread use of multivalent pneumococcal polysaccharides and conjugate vaccines has significantly decreased the incidence of serious IPD, the emergence of vaccine-resistant serotypes that cause IPD is an increasing global problem (Nakano et al., 2016). Therefore, development of alternative therapeutic approaches is urgent and has been hampered by poor characterization of the molecular mechanisms of the intracellular fate of *S. pneumoniae*.

Autophagy is an essential degradation system in eukaryotic cells and plays diverse roles in cellular responses to starvation and removal of damaged organelles and misfolded protein aggregates. Selective autophagy also is an intrinsic defence system against intracellular bacterial pathogens (Galluzzi et al., 2017). In previous studies, we investigated selective autophagy recognition mechanisms for intracellular bacteria, such as *Shigella flexneri* and *Listeria monocytogenes*, and demonstrated that these pathogens are sensed by host cargo receptors (Ogawa et al., 2005; Ogawa et al., 2011; Yoshikawa et al., 2009). Although induction of nonselective autophagy has been associated with the *S. pneumoniae*-derived pore-forming toxin pneumolysin (Ply) and reactive oxygen species (Kim, Paton, Briles, Rhee, & Pyo, 2015; Li et al., 2015), selective autophagy targeting of intracellular *S. pneumoniae* has not been previously demonstrated.

In this study, we demonstrate that intracellular *S. pneumoniae* is subject to selective autophagy via ubiquitin-p62-LC3 cargo and that Rab41 relocated from the Golgi complex to *S. pneumoniae*-containing autophagic vesicles (PcAV) is involved in PcAV biogenesis. Finally, we identified Nedd4-1 as a PcAV-localized essential host factor that plays pivotal roles in the deposition of K63-linked polyubiquitin signal on PcAV and is involved in the efficient formation of PcAV and elimination of intracellular *S. pneumoniae*.

## 2 | RESULTS

### 2.1 | Intracellular *S. pneumoniae* is targeted and eliminated by selective autophagy

To determine the intracellular fate of *S. pneumoniae*, we investigated whether the bacteria are colocalized with LC3, which is an established marker of autophagosomes. In these experiments, baby hamster kidney (BHK) cells stably expressing mCherry-LC3 (for R6) or GFP-LC3 (for TIGR4) were infected with the *S. pneumoniae* strains R6 (unencapsulated highly cell invasive strain) or TIGR4 (encapsulated strain) for 2 hr. Subsequently, mCherry-LC3 or GFP-LC3 was frequently colocalized with intracellular *S. pneumoniae*-containing vacuoles (PCV; Figures 1a upper panel and S1a), suggesting that encapsulated and unencapsulated *S. pneumoniae* are autophagy targets. Capsule dampens pneumococcal adhesion and invasion into host cells, and capsule is downregulated during interaction with host cells (Chao, Marks, Pettigrew, & Hakansson, 2014). Therefore, we, like others in the field (Gradstedt, Iovino, & Bijlsma, 2013; Zhang et al., 2000), used unencapsulated *S. pneumoniae* strain R6 (hereafter referred to as *S. pneumoniae* solely) in this study. LC3-positive PCV (hereafter referred to as PcAV) were also observed in Detroit 562 human nasopharyngeal epithelial cells and mouse embryonic fibroblasts (MEFs) infected with *S. pneumoniae* (Figure 1a, middle and lower), suggesting that *S. pneumoniae* is generally subject to autophagy in nonphagocytic cells. Moreover, populations of PcAV-containing cells among wild-type (WT) MEFs were increased to 53% by 2 hr and were sustained until 3 hr after infection, whereas PcAV were barely detected in autophagy-defective Atg5 knockout (KO) MEFs (Figure 1b). In thin-section electron microscopy experiments, intracellular *S. pneumoniae* was frequently found in double membrane-bound vacuolar compartments in WT cells (Figure 1c, left panel), whereas no such structures containing *S. pneumoniae* were observed in Atg5 KO MEFs (Figure 1c, right panel). Previous studies show that canonical autophagy is impaired in Atg5, Atg7, Atg16L1, FIP200, and ULK1/2 KO MEFs, whereas FIP200 and ULK1/2 are dispensable during LC3-associated phagocytosis (Galluzzi et al., 2017). Thus, to further investigate molecular mechanisms of PcAV formation, we infected WT and various KO MEFs with *S. pneumoniae* for 2 hr and confirmed that PcAV formation is dramatically decreased in the absence of Atg7, Atg16L1, FIP200, and ULK1/2 (Figures 1d and S1b,c). In a recent study, PI3P from type III PI3K complexes was required for induction of LC3-associated phagocytosis and canonical autophagy (Galluzzi et al., 2017). In the present study, WT MEFs infection with *S. pneumoniae* for 2 hr in the presence of

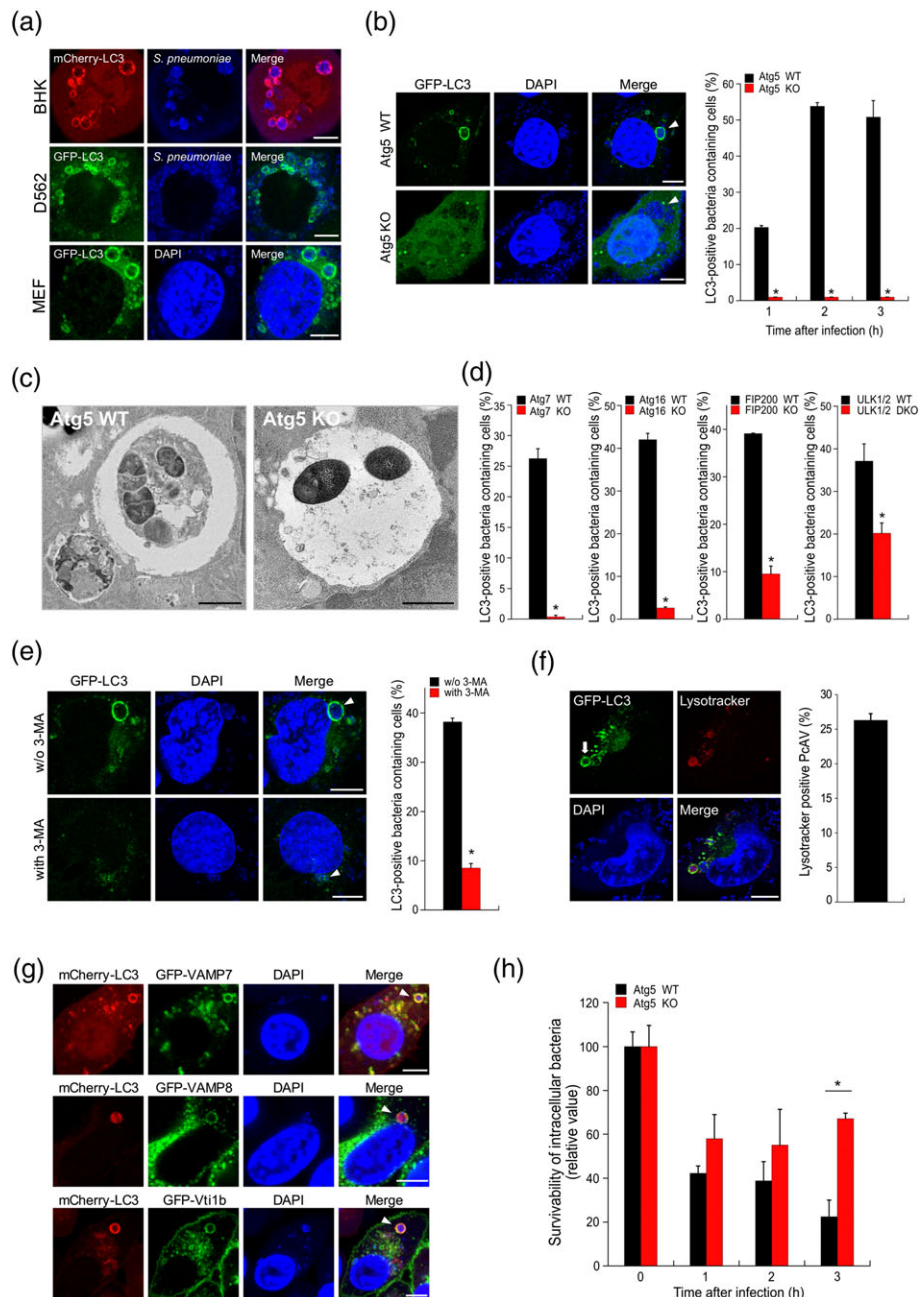


**FIGURE 1** Autophagic degradation of intracellular *Streptococcus pneumoniae*. (a) BHK/mCherry-LC3, D562/GFP-LC3, and wild-type (WT) mouse embryonic fibroblasts (MEFs)/GFP-LC3 were infected with *S. pneumoniae* for 2 hr and were stained with anti-pneumococcus antibody or 4',6-diamidino-2-phenylindole (DAPI; blue); bar, 5  $\mu$ m. (b) Atg5 WT and knockout (KO) MEFs carrying GFP-LC3 were infected with *S. pneumoniae* for 1, 2, or 3 hr and were then stained with DAPI (blue) and percentages of *S. pneumoniae*-containing vesicles (PcAV)-positive cells were quantified. Representative epifluorescence images are shown at 2-hr post infection (p.i.); bar, 5  $\mu$ m. (c) Atg5 WT or KO MEFs were infected with *S. pneumoniae* for 2 hr and were observed using electron microscopy; bar, 1  $\mu$ m. (d) Atg7, Atg16, FIP200, and ULK1/2 WT or KO MEFs expressing GFP-LC3 were infected with *S. pneumoniae* for 2 hr, were stained with DAPI, and percentages of PcAV-positive cells were then quantified. (e) MEFs/GFP-LC3 were infected with *S. pneumoniae* for 2 hr in the presence or absence of 10-mM 3-methyladenine, were stained with DAPI (blue), and percentages of PcAV-positive cells were then quantified. Representative epifluorescence images are shown; bar, 5  $\mu$ m. (f) Atg5 WT MEFs were infected with WT *S. pneumoniae* for 2 hr in the presence of 50-nM LysoTracker and were stained with DAPI (blue), and the percentages of LysoTracker-positive (acidified) PcAV-containing cells were then quantified. Representative epifluorescence images are shown; bar, 5  $\mu$ m. Arrow indicates acidified PcAV. (g) BHK/mCherry-LC3 expressing GFP-VAMP7, -VAMP8, or -Vti1b were infected with *S. pneumoniae* for 2 hr and were stained with DAPI (blue); bar, 5  $\mu$ m. (h) Atg5 WT or KO MEFs were infected with *S. pneumoniae* for indicated periods. Intracellular survivability of bacteria was determined and expressed in colony forming units (cfu);  $n = 3$ . Arrowheads indicate PcAV or PCV; data are expressed as means  $\pm$  standard errors of the mean (SEM); \* $p < .01$

the type III PI3K inhibitor 3-methyladenine (3-MA) decreased populations of PcAV-containing cells from 38% (without 3-MA) to 8.5% (with 3-MA; Figure 1e). Subsequently, we confirmed that

approximately 25% of PcAV are acidified at 2 hr after infection (Figure 1f). Because these results indicate that PcAV are formed by a canonical autophagy system, we examined the association of PcAV

with lysosomes in GFP-VAMP7, -VAMP8, and -Vti1b expressing cells. These soluble N-ethylmaleimide-sensitive factor activating protein receptor (SNARE) proteins play pivotal roles in autophagosomes-lysosomes fusion (Furuta, Fujita, Noda, Yoshimori, & Amano, 2010), and the recruitment of GFP-VAMP7, -VAMP8, and -Vti1b to PcAV was frequently observed after 2 hr of infection (Figure 1g). In addition, at 3 hr after infection, *S. pneumoniae* survival significantly increased in Atg5 KO MEFs (67%) compared with that in WT MEFs (22%; Figure 1h). These results indicate that *S. pneumoniae*-targeted autophagy plays an important role in bacterial clearance.

## 2.2 | Pneumolysin plays pivotal roles in PcAV formation and in the evasion of the lysosomal bactericide during endocytic pathway activation

During infection, *S. pneumoniae* release pore-forming cytolysins known as pneumolysin (Ply; Barnett et al., 2015). We investigated intracellular fates of *ply* mutant *S. pneumoniae* in BHK cells stably expressing mCherry-LC3. At 2-hr post infection (p.i.) with WT or *ply* *S. pneumoniae*, PcAV-containing cell percentages were dramatically lower in *ply* bacteria-infected cells (0.4%) than in WT bacteria-infected cells (41%; Figure 2a). In agreement, LC3-II (activated form

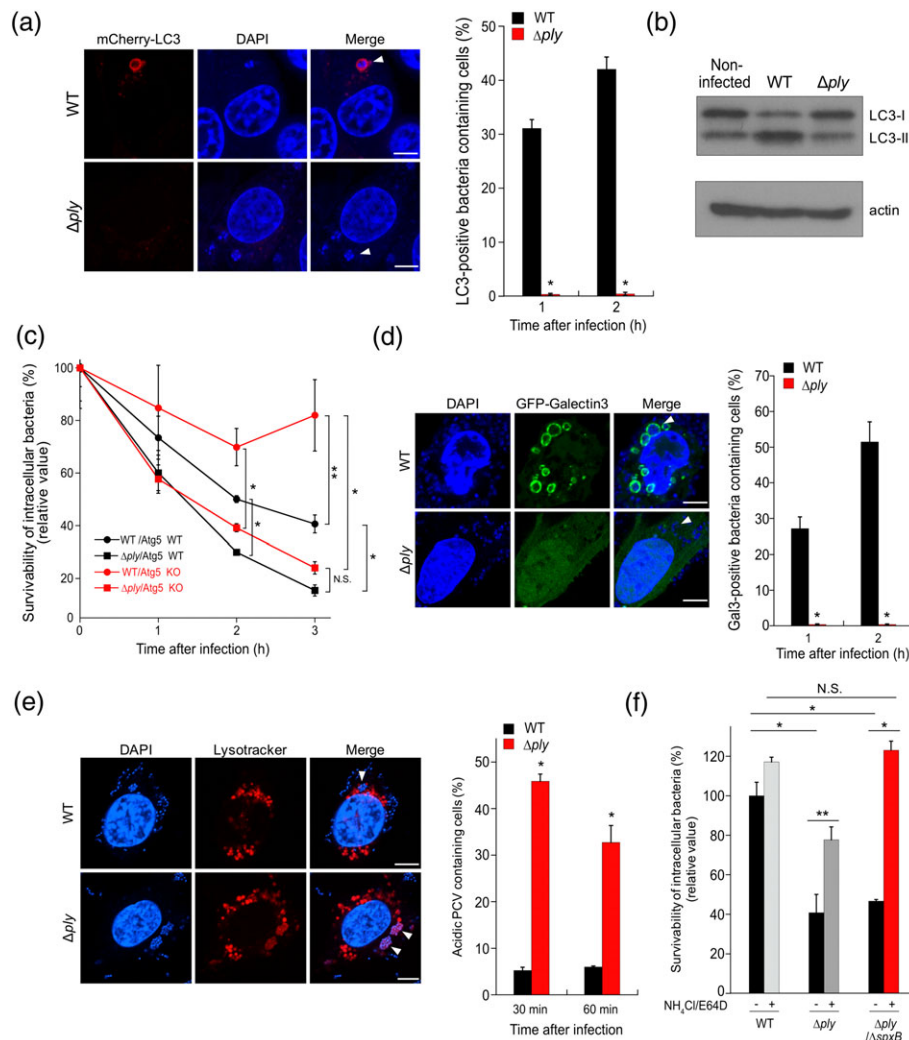


**FIGURE 2** Dual roles of pneumolysin in *Streptococcus pneumoniae*-infected cells. (a) BHK/mCherry-LC3 were infected with wild-type (WT) or *ply* *S. pneumoniae* for 2 hr and were stained with 4',6-diamidino-2-phenylindole (DAPI; blue), and percentages of *S. pneumoniae*-containing vesicles (PcAV)-positive cells were then quantified. Representative epifluorescence images are shown at 2-hr post infection (p.i.); bar, 5  $\mu$ m. (b) WT mouse embryonic fibroblasts (MEFs) were infected with WT or *ply* *S. pneumoniae* for 2 hr, and lysates were subjected to immunoblotting with antibodies against LC3 and actin. (c) Atg5 WT or knockout (KO) MEFs were infected with WT or *ply* *S. pneumoniae* for indicated periods. Intracellular survivability of bacteria was determined and expressed in colony forming units (cfu; n = 3). (d) Atg5 KO MEFs expressing GFP-Galectin3 were infected with WT or *ply* *S. pneumoniae* for 2 hr and were stained with DAPI (blue), and percentages of GFP-Galectin3-positive PCV-containing cells were quantified. Representative epifluorescence images are shown at 2-hr p.i.; bar, 5  $\mu$ m. (e) Atg5 KO MEFs were infected with WT or *ply* *S. pneumoniae* for 2 hr in the presence of 50-nM LysoTracker and were stained with DAPI (blue), and percentages of LysoTracker-positive (acidified) PCV-containing cells were then quantified. Representative epifluorescence images are shown at 30-min p.i.; bar, 5  $\mu$ m. (f) Atg5 KO MEFs were infected with WT, *ply*, or *ply*/ $\Delta$ *SpxB* *S. pneumoniae* for 1 hr in the presence or absence of lysosomal inhibitors (30-mM  $\text{NH}_4\text{Cl}$  and 10- $\mu$ M E64D). Intracellular survivability of bacteria was expressed as colony forming units (cfu; n = 3). Arrowheads indicate PcAV or PCV. Data are presented as means  $\pm$  standard errors of the mean (SEM); \*p < .01, \*\*p < .05; NS, not significant

of LC3) levels and LC3-II/LC3-I ratios were dramatically increased in WT *S. pneumoniae*, but not in *ply*-infected cells (Figures 2b and S2). Based on these results, intracellular survival was expected to be greater for *ply* than for WT *S. pneumoniae*. However, numbers of *ply* *S. pneumoniae* were remarkably lower than those of WT bacteria, even in Atg5 KO MEFs (Figure 2c), suggesting that *S. pneumoniae ply* are eliminated by a host-degradative system other than autophagy.

Because Ply is a pore-forming toxin, we speculated that endosomal membrane damage by Ply may be essential for the subversion of the lysosomal bactericidal system during endocytosis at the early stages of infection. Accordingly, we performed experiments with WT or *ply S. pneumoniae*-infected Atg5 KO MEFs, which were used to eliminate autophagic bactericidal effects. In subsequent analyses, cell populations containing PCV and the marker of damaged endosomal membranes GFP-Galectin3, a lectin protein that can bind to  $\beta$ -galactose-containing glycoconjugates on the cell surface and in the lumens of endosomes, were dramatically lower in *ply S. pneumoniae*-infected cells (0.4%) than in those infected with the WT strain (50%; Figure 2d). Because bacterial pore-forming cytolysin was previously identified as a suppressor of endosome acidification (Beaugard, Lee, Collier, & Swanson, 1997; Henry et al., 2006; Lu et al., 2015), we compared percentages of acidic PCV-containing Atg5 KO MEFs following WT and *ply S. pneumoniae* infection and observed dramatically lower acidification in WT bacteria-infected cells than in *ply* bacteria-infected cells (Figure 2e). Subsequently, we performed recovery assays to determine *S. pneumoniae ply* survival in the presence of lysosomal inhibitors. In these experiments, the inhibitors NH<sub>4</sub>Cl and E64d led to partial recovery of *ply* bacteria in Atg5 KO MEFs (Figure 2f). Previously, a pneumococcal pyruvate oxidase (SpxB) was identified in *S. pneumoniae* as a source of hydrogen peroxide (H<sub>2</sub>O<sub>2</sub>), although high concentrations of H<sub>2</sub>O<sub>2</sub> are known to cause bacterial cell lysis (Regev-Yochay, Trzcinski, Thompson, Lipsitch, & Malley, 2007). Therefore, we performed recovery assays with a *ply/ΔspxB* bacterial strain in the presence of lysosomal inhibitors (Figure 2f) and showed complete recovery of the *ply/ΔspxB* strain to WT levels. Although *spxB*-depletion reportedly affects the production of H<sub>2</sub>O<sub>2</sub> and intrabacterial acetyl-CoA production (Echlin et al., 2016), these data suggest that *S. pneumoniae ply* is mainly eliminated by lysosomal enzymes and partially by self-derived H<sub>2</sub>O<sub>2</sub> in PCV.

### 2.3 | Ubiquitin-p62-LC3 cargo is involved in *S. pneumoniae*-targeted autophagy

Because autophagy cargo receptors such as p62, NDP52, and optineurin are recruited to invading pathogens and pathogen-containing vacuoles (Fujita et al., 2013; Galluzzi et al., 2017; Yoshikawa et al., 2009), we determined p62 and polyubiquitin (poly-Ub) recruitment to PcAV in *S. pneumoniae*-infected cells. When BHK/mCherry-LC3 or WT MEFs/GFP-LC3 were infected with WT *S. pneumoniae*, poly-Ub and p62 signals were frequently detected around PcAV, whereas no recruitment of these molecules was observed after infection with Ply mutant bacteria (Figure 3a,b). These data indicate that membrane damage by Ply is a prerequisite for recruitment of poly-Ub and p62. Moreover, treatment with the E1 inhibitor PYR-41 during infection led to dramatic decreases in numbers of poly-Ub, p62-, and LC3-

positive PCV (Figures 3c and S3a), suggesting that poly-Ub deposition on PCV is a prerequisite for p62 recruitment to PCV, and for PcAV formation. In further experiments, we investigated the relationship between autophagic activity and poly-Ub deposition on PCV and showed no significant differences in poly-Ub recruitment around PCV in Atg5 WT and KO MEFs at 1-hr p.i., but significant autophagy dependent decreases in poly-Ub signals at 2-hr p.i. These data further confirm that ubiquitinated PCV are degraded by autophagy (Figures 3d and S3b). Moreover, after infection of p62 WT and KO MEFs with *S. pneumoniae*, numbers of PcAV-positive cells were significantly lower in p62 KO MEFs than WT MEFs (Figure 3e), suggesting that p62 is required for PcAV formation. The recruitment of an autophagy receptor NDP-52 to PcAV was significantly lower than that of p62 (Figure 3b,c,f), and NDP-52-recruitment to PcAV was abolished in p62 KO MEF (Figure 3f), suggesting that p62 is a primary autophagy cargo during the formation of PcAV. Numbers of ubiquitinated PCV-positive cells were also remarkably lowered in p62 KO MEFs (Figure 3g), indicating that p62 enhances poly-Ub deposition on PcAV (see below). The cargo receptor p62 contains a PB1 domain at its N-terminal, an LC3-interacting region (LIR) in the middle portion, and a ubiquitin-associated (UBA) domain at its C-terminal (Figure 3h, inset). To identify which of these domains are responsible for recruitment of p62 and LC3 to PCV, we generated a series of p62-3 × Myc deletion mutants lacking LIR, UBA, or both domains ( $\Delta$ LIR/ $\Delta$ UBA), or containing two amino-acid substitutions (K7A/D69A) in the PB1 domain that prevent p62 multimerisation (Figure 3h). After stably expressing these proteins in p62 KO MEFs, PcAV formation was significantly decreased in p62 KO MEFs expressing  $\Delta$ UBA,  $\Delta$ LIR, or  $\Delta$ UBA/ $\Delta$ LIR, indicating that poly-Ub-p62 and p62-LC3 interactions are required for PcAV formation (Figure 3h). Moreover, PcAV formation was partially recovered in p62 KO MEFs expressing K7A/D69A, and hence, the PB1 domain of p62 likely enhances PcAV formation. In further experiments, numbers of p62-positive PCV were significantly decreased in p62 KO MEFs expressing  $\Delta$ UBA,  $\Delta$ UBA/ $\Delta$ LIR, or K7A/D69A (Figure 3h). Intriguingly, p62 recruitment to PCV was not fully recovered by  $\Delta$ LIR in this system, indicating that interaction of the p62 LIR domain with LC3 enhances associations of p62 with PcAV (see discussion).

### 2.4 | Golgi-derived Rab41 is recruited to PcAV and involved in PcAV formation

To comprehensively screen for Rab proteins that are associated with *S. pneumoniae*-targeting autophagosomes, we expressed EGFP-tagged mouse Rab proteins (Rabs) in BHK/mCherry-LC3 cells and investigated colocalization of GFP-Rabs with PcAV at 2 hr after infection with *S. pneumoniae*. At this time point, *S. pneumoniae* autophagy plateaus, and among 58 Rabs, Rab15, 19, 27A, 27B, 29, 32, 38, 41, and 42 were clearly recruited to PcAV (Figure S4a). In addition, Rab15, 19, 38, 41, and 42 were also clearly recruited to PcAV in MEFs (Figure 4a). In subsequent experiments, we examined the recruitment of these Rabs to PCV in Atg5 KO MEFs. Although Rab38 and 42 were recruited to PCV independently of autophagy, Rabs15, 19, and 41 were recruited only in Atg5 WT MEFs. Moreover, siRNA-mediated knockdown (KD) of Rabs15, 19, 38, 41, and 42 led to clear reductions

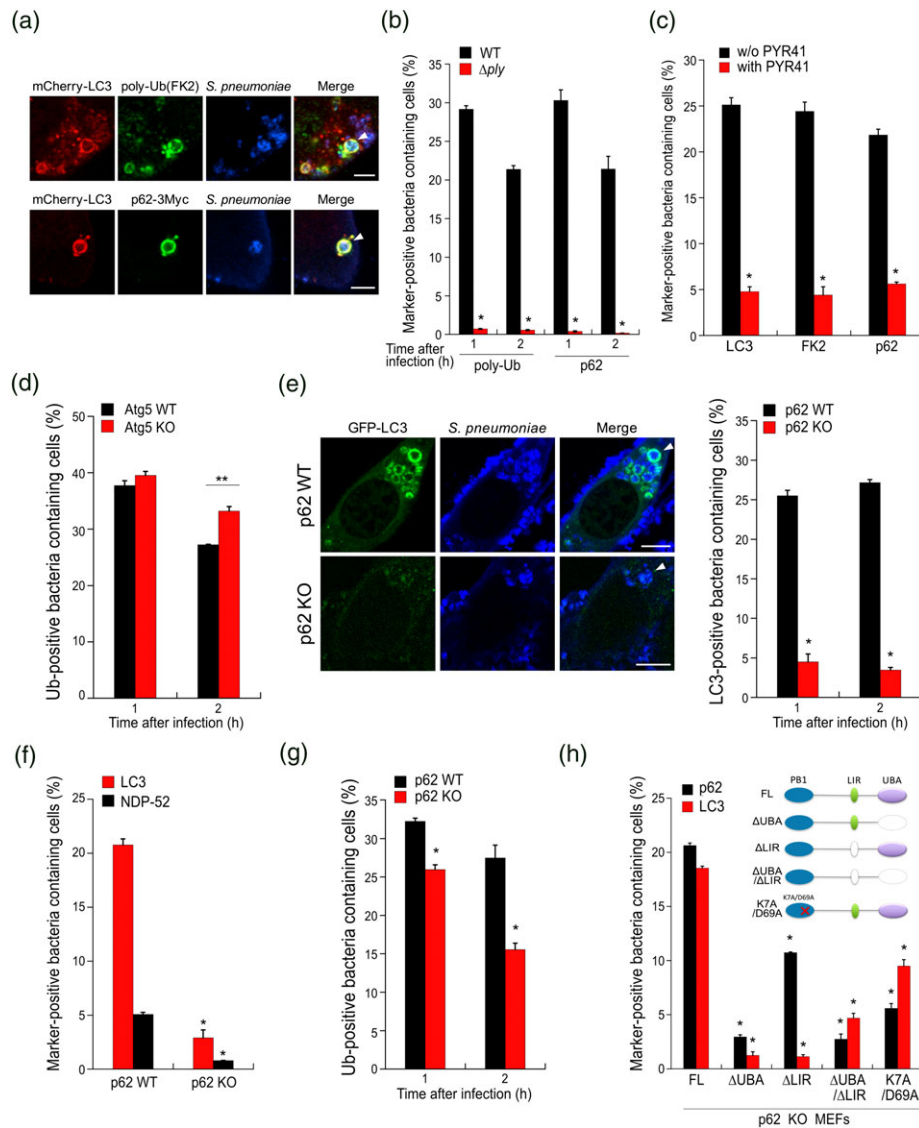


**FIGURE 3** Ub-p62-LC3 cargo is involved in *Streptococcus pneumoniae*-containing vesicles (PcAV) formation. (a) BHK/mCherry-LC3 or BHK/mCherry-LC3 expressing p62-3Myc was infected with wild-type (WT) *S. pneumoniae* for 2 hr and were stained with anti-*S. pneumoniae*, and -poly-Ub or -Myc antibodies; bar, 5  $\mu$ m. (b) WT mouse embryonic fibroblasts (MEFs)/GFP-LC3 were infected with WT or *ply* *S. pneumoniae* for 2 hr and were stained with 4',6-diamidino-2-phenylindole (DAPI) and antibodies against poly-Ub or p62, and percentages of poly-Ub- or p62-positive PcAV (WT) or PCV (*ply*)-containing cells were then quantified. (c) WT MEFs/GFP-LC3 were infected with WT *S. pneumoniae* for 2 hr in the presence or absence of 30- $\mu$ M PYR-41 and were stained with DAPI and antibodies against poly-Ub or p62, and percentages of poly-Ub- or p62-positive PcAV or PCV-containing cells were then quantified. (d) Atg5 WT or knockout (KO) MEFs/mCherry-LC3 were infected with *S. pneumoniae* for 2 hr and were stained with DAPI (blue) and anti-poly-Ub antibody, and percentages of poly-Ub-positive PcAV or PCV-containing cells were then quantified. (e) p62 WT or KO MEFs/GFP-LC3 were infected with *S. pneumoniae* for 2 hr and were stained with anti-*S. pneumoniae* antibody, and percentages of PcAV-positive cells were then quantified. Representative epifluorescence images are shown; bar, 5  $\mu$ m. (f) p62 WT or KO MEFs/mCherry-LC3/GFP-NDP52 were infected with *S. pneumoniae* for 2 hr and were then stained with DAPI, and percentages of LC3- or NDP52-positive PcAV- or PCV-containing cells were quantified. (g) p62 WT or KO MEFs/GFP-LC3 were infected with *S. pneumoniae* for 2 hr and were stained with DAPI and anti-poly-Ub antibody, and percentages of poly-Ub-positive PcAV or PCV-containing cells were quantified. (h; inset) Schematic of p62-3xmyc; p62 KO MEFs/GFP-LC3/p62-3xmyc (WT,  $\Delta$ LIR,  $\Delta$ UBA,  $\Delta$ LIR- $\Delta$ UBA, K7A/D69A) were infected with *S. pneumoniae* for 2 hr and were stained with DAPI and anti-Myc antibody, and percentages of LC3- or p62-positive PCV-containing cells were then quantified. Arrowheads indicate PcAV or PCV. Data are presented as means  $\pm$  standard errors of the mean (SEM); \* $p$  < .01, \*\* $p$  < .05

in numbers of PcAV-containing cells (Figure 4b), and intracellular survivability of *S. pneumoniae* (Figure 4c) was increased in Rab38, 41, and 42 KD cells, and the effect was remarkable in Rab41 KD cells. Therefore, we analysed associations of Rab41 and *S. pneumoniae*-induced autophagy and observed time-dependent increases in the number of Rab41-positive PcAV-containing cells (Figure 4d). In further experiments, GFP-Rab41 was characteristically localized with PcAV and at

PcAV-PcAV contact sites (Figure 4e). Thus, to elucidate mechanisms of Rab41 recruitment to PCV and PcAV, we determined numbers of GFP-Rab41-positive bacteria in *ply S. pneumoniae*-infected cells and observed very few Rab41-positive PCV (Figure 4f). Similarly, numbers of Rab41-positive PCV-containing cells were dramatically decreased in Atg5 and p62 KO MEFs (Figures 4g,h, and S4b). No differences in the perinuclear localization of Rab41 were identified between noninfected

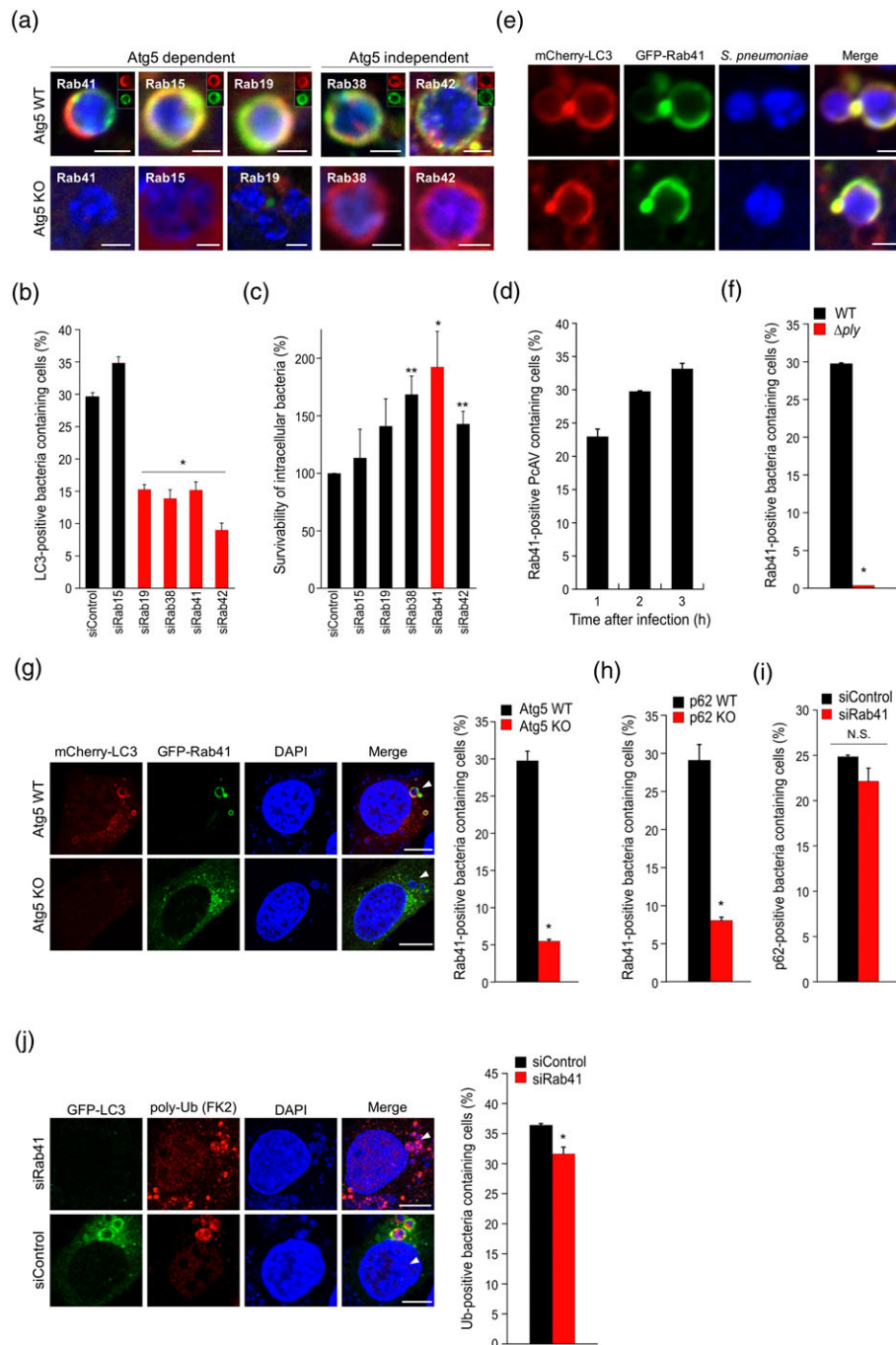


**FIGURE 4** Rab41 is localized on *Streptococcus pneumoniae*-containing vesicles (PcAV) and is involved in PcAV formation. (a) Atg5 wild-type (WT) or knockout (KO) mouse embryonic fibroblasts (MEFs)/GFP-LC3 expressing mStrawberry-Rab15, 19, 38, 41, or 42 were infected with *S. pneumoniae* for 2 hr and were stained with anti-*S. pneumoniae* antibody (blue); bar, 2  $\mu$ m. (b) WT MEFs/mCherry-LC3 were treated with indicated siRNAs, were infected with *S. pneumoniae* for 2 hr and stained with 4',6-diamidino-2-phenylindole (DAPI), and percentages of PcAV-containing cells were then quantified. (c) WT MEFs were treated with indicated siRNAs and were infected with *S. pneumoniae* for 2 hr. Intracellular survivability of bacteria was determined and expressed as colony forming unit (cfu;  $n = 3$ ). (d) WT MEFs/GFP-Rab41 were infected with *S. pneumoniae* for indicated periods and were stained with DAPI, and percentages of GFP-Rab41-positive PcAV were then quantified. (e) BHK/mCherry-LC3 expressing GFP-Rab41 was infected with *S. pneumoniae* for 2 hr and were stained with anti-*S. pneumoniae* antibody (blue); bar, 2  $\mu$ m. (f) WT MEFs/GFP-Rab41 were infected with WT or *ply* *S. pneumoniae* for 2 hr and were stained with DAPI, and percentages of GFP-Rab41-positive PCV-containing cells were then quantified. (g) Atg5 WT or KO MEFs/GFP-Rab41 infected with *S. pneumoniae* for 2 hr and were stained with DAPI, and percentages of GFP-Rab41-positive PcAV or PCV-containing cells were then quantified. Representative epifluorescence images are shown; bar, 5  $\mu$ m. (h) p62 WT or KO MEFs/GFP-Rab41 were infected with *S. pneumoniae* for 2 hr and were stained with DAPI, and percentages of GFP-Rab41-positive PcAV or PCV-containing cells were then quantified. (i) WT MEFs/GFP-LC3 were treated with siRab41, were infected with *S. pneumoniae* for 2 hr, and were stained with DAPI and anti-p62 antibodies, and percentages of p62-positive PcAV or PCV-containing cells were then quantified. (j) WT MEFs/GFP-LC3 were treated with siRab41, were infected with *S. pneumoniae* for 2 hr, and were stained with DAPI and anti-poly-Ub antibody, and percentages of poly-Ub-positive PcAV or PCV-containing cells were then quantified. Representative epifluorescence images are shown; bar, 5  $\mu$ m. Arrowheads indicate PcAV or PCV; data are presented as means  $\pm$  standard errors of the mean (SEM); \* $p < .01$ , \*\* $p < .05$ ; NS, not significant

Atg5 WT and KO MEFs (Figure S4c). These results showed that PcAV formation is prerequisite for the recruitment of Rab41 around invaded *S. pneumoniae*. We next investigated whether Rab41-KD influences poly-Ub or p62 recruitment to PCV. After confirming KD efficiency using reverse transcriptase-polymerase chain reaction (RT-PCR) analyses (Figure S4d), Rab41 KD had almost no or slight effects on the recruitment of p62 and poly-Ub to PCV (Figure 4i,j), suggesting limited roles of Rab41 in cargo-receptor recruitment at the early stages of autophagic recognition.

## 2.5 | Rab41-positive intact Golgi complexes are prerequisite for PcAV formation

To investigate the roles of Rab41 in PcAV formation, we generated WT MEFs stably expressing WT Rab41, CA (Q75L, GTP-locked form), and CN (T30N, GDP-locked form). In subsequent experiments, no significant differences in PcAV formation were observed between Rab41 WT and CA expressing cells, whereas Rab41 CN expression remarkably reduced numbers of PcAV-containing cells (Figure 5a,b, left). Furthermore, Rab41 CN recruitment to PcAV was dramatically suppressed compared with Rab41 WT recruitment. Moreover, Rab41 CA recruitment to PcAV was slightly increased (Figure 5a,b, right), indicating that the GTP binding is required for Rab41 recruitment to PcAV and for efficient PcAV formation. Rab41 is a Golgi-resident protein that plays roles in ER-Golgi trafficking (Haas et al., 2007). Accordingly, in noninfected MEFs, GFP-Rab41 was localized to perinuclear GM130-positive Golgi apparatuses. However, most GFP-Rab41 signals were translocated from the Golgi to PcAV, and Rab41-positive PcAV were frequently colocalized with GM130 in *S. pneumoniae*-infected cells (Figure 5c), suggesting that PcAV membranes originate in part from Golgi complexes. We also determined colocalization of host Golgi- or ERGIC located proteins, such as Golgin-97, COG6, ERGIC53, and Sec22b with PcAV. As shown in Figure 5d, the trans-Golgi network resident protein Golgin-97 was colocalized with Rab41 at perinuclear regions, but the other markers were not colocalized with PcAV (Figure 5d). Thus, to investigate the recruitment of Rab41 to canonical autophagosomes, we examined localizations of GFP-Rab41 in MEFs/mCherry-LC3/GFP-Rab41 cells. After treatments with the rapamycin, a canonical autophagy inducer, mCherry-LC3 puncta formation was dramatically induced; however, most GFP-Rab41 staining remained in perinuclear regions, and little colocalization of GFP-Rab41 with mCherry-LC3 puncta was detected (Figure 5e). Thus, to confirm the requirement of Rab41 for PcAV formation, we generated Rab41-deficient MEFs using a CRISPR/Cas9 genome editing system (Figure S5a). In accordance with previous reports using Rab41-KD cells, Rab41 KO caused Golgi fragmentation (Figure 5f,h). Therefore, we checked canonical autophagy responses in Rab41 WT and KO MEFs using Western blotting. Although background autophagic activity was slightly decreased in Rab41 KO MEFs, rapamycin-induced autophagy responses and autophagy flux were normal in Rab41 KO MEFs (Figure S5b). In contrast, Rab41 deficiency significantly limited the formation of PcAV (Figure 5i), indicating the requirement of intact Golgi complex structures for PcAV formation. Accordingly, treatments of WT MEFs with Brefeldin A (BFA), a well-established Golgi

toxin, had similar inhibitory effects on PcAV formation (Figure 5j), thereby suggesting the involvement of structural integrity of Golgi apparatus in PcAV formation. Notably, LAMP-1 recruitment to PCV was normal in Rab41 KO MEFs (Figure S5c).

## 2.6 | Ned4-1-mediated K63Ub-linked chain formation is involved in PcAV biogenesis

To further investigate the intracellular fate of *S. pneumoniae*, we identified types of polyubiquitination signals on PcAV using indirect immunofluorescence staining with chain-specific antibodies. Because associations of the UBA domain of p62 with both K48- and K63-linked polyubiquitin chains were characterized previously (Haldar et al., 2015), we compared K48- and K63-linked polyubiquitin chain deposition on PCV in WT and Atg5 KO MEFs. In Atg5 WT MEFs, PcAV with K48-linked polyubiquitin chain (K48Ub) signals were decreased from 31% at 1-hr p.i. to 15% at 2-hr p.i. However, these were not decreased in Atg5 KO MEFs (Figures 6a and S6a), indicating that the K48Ub-positive substrate was degraded by autophagy and that K48Ub-modification continues even in Atg5 KO MEFs. In contrast, numbers of K63-linked polyubiquitin chain (K63Ub)-positive PCV were not decreased with the progress of infection, even in Atg5 WT MEFs (19% at 1-hr p.i. to 20% at 2-hr p.i.), and K63Ub modification was dramatically decreased to <5% in Atg5 KO MEFs (Figures 6a and S6a). In agreement with the data in Figure 3d, numbers of FK2 (antibody against all types of polyubiquitin chains)-positive bacteria were increased in Atg5 KO MEFs (Figure 6a). Moreover, K48Ub signals were mostly detected inside PcAV, whereas K63Ub signals were mostly associated with PcAV membranes (Figures 6b and S6a). Next, we examined polyubiquitin types that are localized with PCV (or PcAV) in p62 WT and KO MEFs. Numbers of FK2-, K48Ub-, and K63Ub-positive PCV in p62 KO MEFs were all decreased, and reductions in K63Ub- and FK2-positive PCV were remarkable (Figure 6c). In contrast, M1-linked linear type ubiquitin chain-specific signals were hardly detected in p62 WT and KO MEFs (Figure 6c). Thus, we determined whether interactions of the p62 UBA domain with ubiquitin and the p62 LIR domain with LC3 influenced the recruitment of K48Ub or K63Ub to PCV, but showed no significant differences in numbers of K48Ub-positive PCV in p62 KO MEFs expressing p62 FL,  $\Delta$ UBA, or  $\Delta$ LIR (Figure 6d). In contrast, numbers of K63Ub-positive PCV in p62 KO MEFs expressing p62  $\Delta$ UBA or  $\Delta$ LIR were significantly reduced to about 45% of that in p62 KO/p62 FL MEFs (Figure 6d). These results show that p62-ubiquitin and p62-LC3 interactions enhance K63Ub recruitment to PcAV. To elucidate mechanisms of K63Ub deposition in PcAV, we investigated PcAV recruitment of E3 ligases that were previously associated with xenophagy. In the ensuing experiments, Keap1, PARK2, LRSAM1, TRIM16, Smurf1, and TRAF6 proteins were not colocalized with PcAV (Figure S6b). Furthermore, PcAV formation and K63Ub recruitment to PcAV were unchanged in TRAF6 KO MEFs (Figure S6c). Because the major E2-conjugating enzyme Ubc13 contributes to the synthesis of K63Ub, we examined PcAV formation in Ubc13 WT and KO MEFs, but observed normal PcAV formation and recruitment of K63Ub to PcAV in Ubc13 KO MEFs (Figures 6e and S6d,e). Subsequently, we examined PcAV recruitment of the HECT ubiquitin E3 ligase family



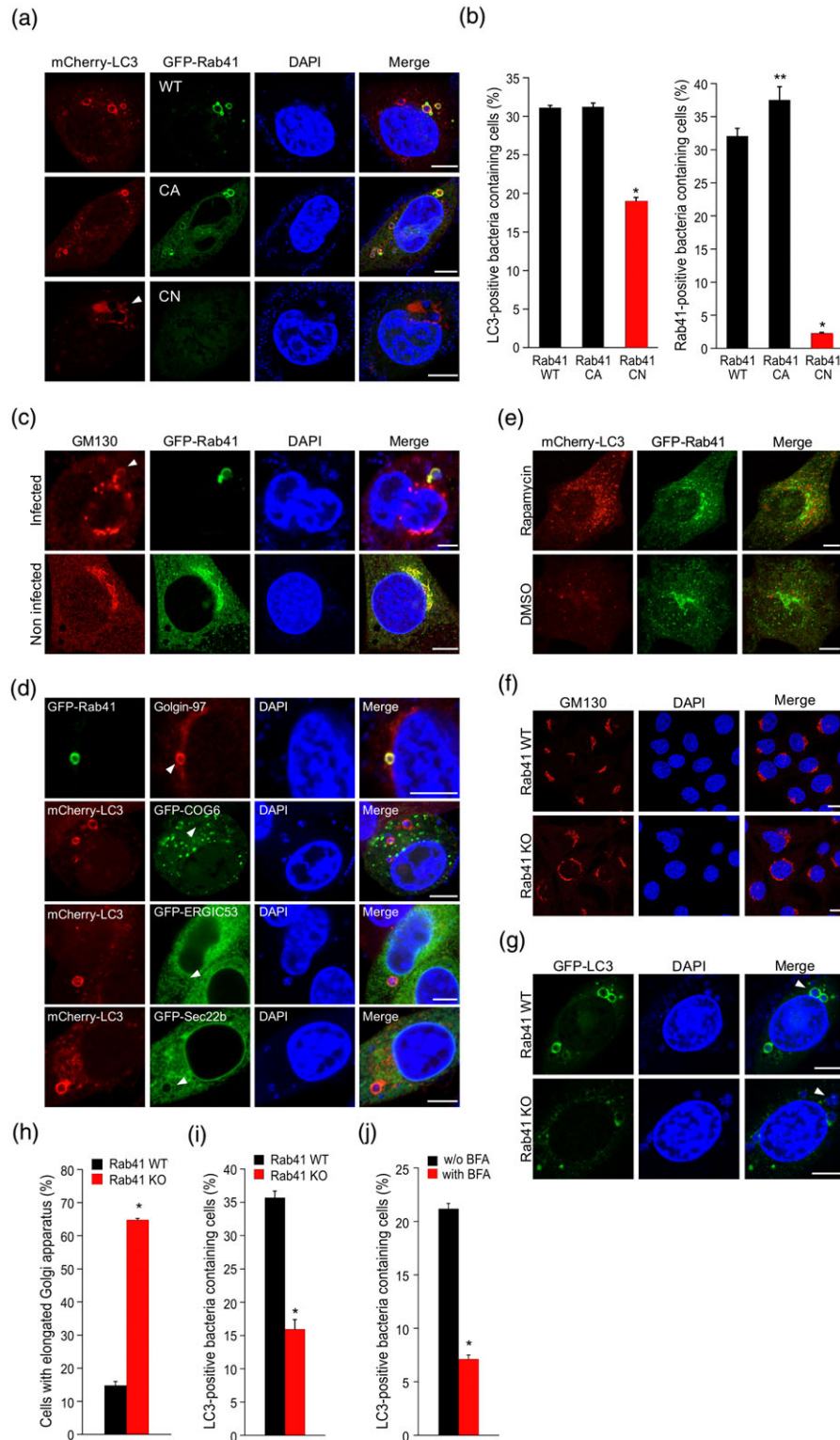


**FIGURE 5** Rab41-resided Golgi apparatus is involved in *Streptococcus pneumoniae*-containing vesicles (PcAV) formation. (a) Wild-type (WT) mouse embryonic fibroblasts (MEFs)/mCherry-LC3 stably expressing GFP-Rab41 WT, CA (Q75L), or CN (T30N) were infected with *S. pneumoniae* for 2 hr and were stained with 4',6-diamidino-2-phenylindole (DAPI); bar, 5  $\mu$ m. (b) Percentages of PcAV-containing cells and GFP-Rab41-positive PcAV or PCV-containing cells in (a) were quantified. (c) WT MEFs/GFP-Rab41 were infected with *S. pneumoniae* for 2 hr and were stained with DAPI and anti-GM130 antibody; bar, 5  $\mu$ m. (d) WT MEFs/GFP-Rab41 or WT MEFs/mCherry-LC3 expressing GFP-COG6, -ERGIC53, or -Sec22b were infected with *S. pneumoniae* for 2 hr and were stained with DAPI and anti-golgin-97 antibody (WT MEFs/GFP-Rab41); bar, 5  $\mu$ m. (e) WT MEFs/mCherry-LC3/GFP-Rab41 were cultured for 2 hr in the presence or absence of 10- $\mu$ M rapamycin; bar, 5  $\mu$ m. (f, h) Rab41 WT or knockout MEFs were stained with DAPI and anti-GM130 antibody (f), and percentages of fragmented Golgi-containing cells were then quantified (h); bar, 5  $\mu$ m. (g, i) Rab41 WT or knockout MEFs/GFP-LC3 were infected with *S. pneumoniae* for 2 hr and were stained with DAPI (g), and percentages of PcAV-containing cells were then quantified (i); bar, 5  $\mu$ m. (j) WT MEFs/GFP-LC3 were infected with *S. pneumoniae* for 2 hr in the presence or absence of 5  $\mu$ g/ml of BFA and were stained with DAPI, and percentages of PcAV-containing cells were then quantified. Arrowheads indicate PcAV or PCV; data are presented as means  $\pm$  standard errors of the mean (SEM); \* $p$  < .01, \*\* $p$  < .05

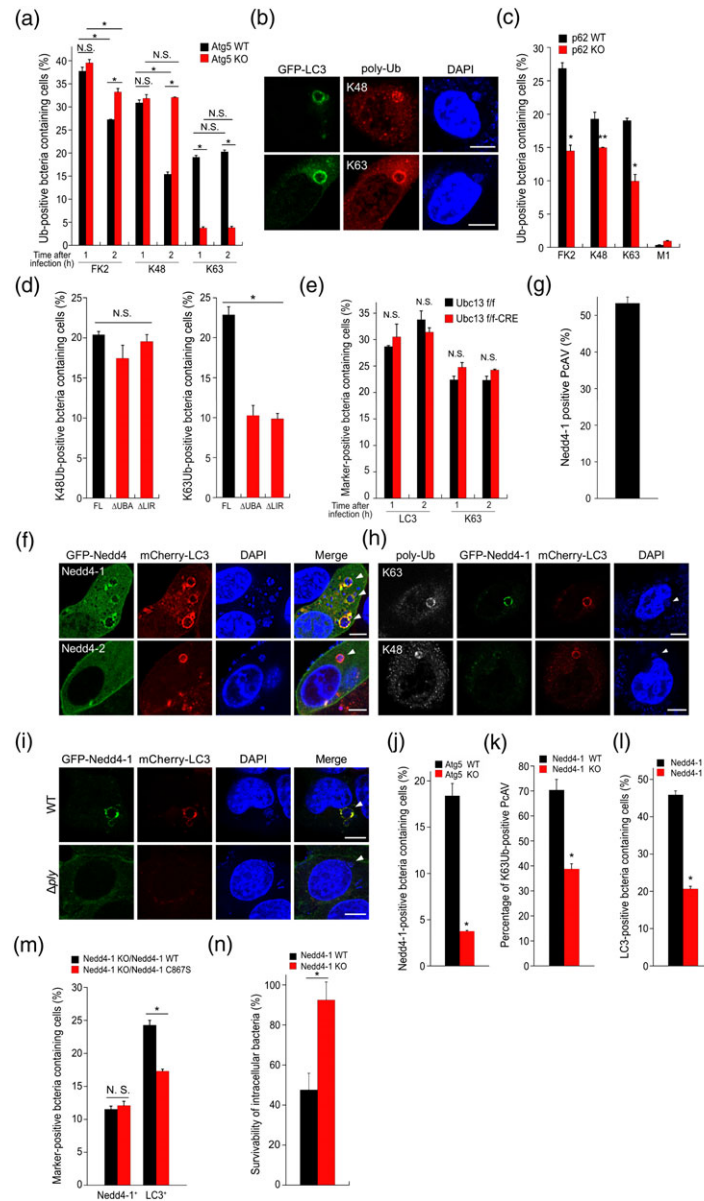


**FIGURE 6** Nedd4-1 mediated K63 Ub is involved in *Streptococcus pneumoniae*-containing vesicles (PcAV) formation. (a) Atg5 wild-type (WT) or knockdown (KO) mouse embryonic fibroblasts (MEFs)/GFP-LC3 were infected with *S. pneumoniae* for indicated periods and were stained with 4',6-diamidino-2-phenylindole (DAPI) and anti-polyubiquitin (FK2, K48, or K63) antibodies, and percentages of each type of Ub-positive PcAV or PCV-containing cells were then quantified. (b) WT MEFs/GFP-LC3 were infected with *S. pneumoniae* for 2 hr and were stained with DAPI (blue) and anti-K48Ub or -K63Ub antibodies; bar, 5  $\mu$ m. (c) p62 WT or KO MEFs/GFP-LC3 were infected with *S. pneumoniae* for 2 hr and were stained with DAPI and anti-polyubiquitin (FK2, K48, K63, or M1) antibodies, and percentages of each type of Ub-positive PcAV or PCV-containing cells were then quantified. (d) p62 KO MEFs/GFP-LC3/p62-3xmyc (FL,  $\Delta$ UBA, or  $\Delta$ LIR) were infected with *S. pneumoniae* for 2 hr and were stained with DAPI and anti-K48Ub or -K63Ub antibodies, and percentages of K48Ub- or K63Ub-positive PCV or PcAV-containing cells were then quantified. (e) Ubc13 WT or KO MEFs/GFP-LC3 were infected with *S. pneumoniae* for 2 hr and were stained with DAPI and anti-K63Ub antibodies, and percentages of PcAV or K63Ub-positive PcAV-containing cells were then quantified. (f) BHK/mCherry-LC3 expressing GFP-Nedd4-1 or -Nedd4-2 were infected with *S. pneumoniae* for 2 hr and were stained with DAPI (blue); bar, 5  $\mu$ m. (g) WT MEFs/GFP-Nedd4-1 were infected with *S. pneumoniae* for 2 hr and were stained with DAPI, and percentages of GFP-Nedd4-1-positive PcAV were then quantified. (h) WT MEFs/mCherry-LC3/GFP-Nedd4-1 were infected with *S. pneumoniae* for 2 hr and were stained with DAPI (blue) and anti-K48Ub or -K63Ub antibodies; bar, 5  $\mu$ m. (i) WT MEFs/mCherry-LC3/GFP-Nedd4-1 were infected with WT or *ply* *S. pneumoniae* for 2 hr and were stained with DAPI (blue); bar, 5  $\mu$ m. (j) Atg5 WT or KO MEFs/mCherry-LC3/GFP-Nedd4-1 were infected with *S. pneumoniae* for 2 hr and were stained with DAPI, and percentages of GFP-Nedd4-1-positive PCV or PcAV-containing cells were then quantified. (k) Nedd4-1 WT or KO MEFs/GFP-LC3 were infected with *S. pneumoniae* for 2 hr and were stained with DAPI and anti-K63Ub antibody, and percentages of K63Ub-positive PcAV were then quantified. (l) Nedd4-1 WT or KO MEFs/GFP-LC3 were infected with *S. pneumoniae* for 2 hr and were stained with DAPI, and percentages of PcAV-containing cells were then quantified. (m) Nedd4-1 WT or KO MEFs/GFP-LC3/FLAG-Nedd4-1 WT or C867S (E3 ligase dead) were infected with *S. pneumoniae* for 2 hr and were stained with DAPI, and percentages of Nedd4-1 or LC3-positive PCV containing cells were then quantified. (n) Nedd4-1 WT or KO MEFs were infected with *S. pneumoniae* for 2 hr. Intracellular survivability of bacteria was determined and expressed in colony forming units ( $n = 3$ ). Arrowheads indicate PcAV. Data are presented as means  $\pm$  standard errors of the mean (SEM); \* $p < .01$ , \*\* $p < .05$ ; NS, not significant

members Nedd4-1 and -2, which synthesise K63Ub without Ubc13. Experiments in *S. pneumoniae*-infected cells showed intensive GFP-Nedd4-1 signals on PcAV, whereas GFP-Nedd4-2 signals were barely detectable (Figure 6f). Moreover, in MEFs stably expressing GFP-Nedd4-1, 53.3% of PcAV were associated with GFP-Nedd4-1 (Figure 6g), and peripheral colocalization of GFP-Nedd4-1 and K63Ub signals was observed on PcAV (Figure 6h). The associations of GFP-Nedd4-1 with PCV (or PcAV) were also dramatically decreased in *ply* *S. pneumoniae*-infected Atg5 WT MEFs and in WT *S. pneumoniae*-infected Atg5 KO MEFs (Figure 6i,j). Subsequently, we investigated the percentage of K63Ub-positive PcAV and number of PcAV-containing cells in Nedd4-1-deficient MEFs and found that K63Ub deposition on PcAV and PcAV formation were significantly decreased in Nedd4-1-deficient MEFs (Figure 6k,l). In addition, when Nedd4-1 KO MEFs/GFP-LC3/Nedd4-1 WT or E3 ligase dead (C867S) was infected with *S. pneumoniae*, the associations of Nedd4-1 with PCV (or PcAV) remained, whereas PcAV formation was clearly decreased in Nedd4-1 KO MEFs/Nedd4-1 C867S (Figure 6m). Finally, *S. pneumoniae* survival significantly increased in Nedd4-1 KO MEFs compared with that in WT MEFs at 2 hr after infection (Figure 6n). Taken all these data, we concluded that Nedd4-1-mediated K63Ub formation on PcAV plays crucial roles in the recruitment of autophagosomal components, the promotion of PcAV formation, and the elimination of *S. pneumoniae* from host cells (e.g., LC3).

### 3 | DISCUSSION

In this study, we investigated intracellular fates of *S. pneumoniae* and focused on mechanisms of selective autophagy for *S. pneumoniae*. The present data show that *S. pneumoniae* is entrapped and degraded by p62-driven selective autophagy within 2–3 hr of infection and that Rab41-positive intact Golgi apparatuses are required for PcAV formation (Figure 7). Finally, we found evidence that supports the notion that Nedd4-1-mediated K63Ub deposition on PcAV acts as a scaffold for PcAV biogenesis (Figure 7).

In previous reports, we demonstrated mechanisms of recognition for selective autophagy of intracellular *S. flexneri* and *L. monocytogenes* (Ogawa et al., 2005; Ogawa et al., 2011; Yoshikawa et al., 2009). In this study, we extended these findings to *S. pneumoniae*, which is a major human pathogen that causes severe invasive infections such as meningitis. Specifically, we showed that this bacterium is selectively engulfed in autophagosomes and analysed the mechanisms behind PcAV formation in terms of interactions between intracellular pneumococcus and host membrane trafficking. As shown in Figure 1, invading *S. pneumoniae* are autophagocytosed in various cell types, and this autophagy is induced in a canonical fashion and is mediated by Atg5, 7, and 16, FIP200, ULK1/2, and PI3P.

The bacterial protein Ply is a cholesterol-binding, thiol-activated cytolysin and is classified in the same family as LLO from *L. monocytogenes* and SLO from Group A streptococcus (GAS; Barnett et al., 2015). Bacterial pore-forming toxins have various effects and induce inflammation, cell death, reactive oxygen species production, cytosolic aggregation, and autophagy during bacterial infection (Barnett et al., 2015). Herein, we show that Ply provides advantages

for bacteria and facilitates escape from endosomal elimination at early stages of infection (Figure 7). However, membrane remnants generated by Ply and cytosolic-exposed bacterial surface proteins are concomitant targets of selective autophagy (Figures 2, 3, and 7). Similarly, SLO in GAS prevents the acidification of phagolysosomes to promote intracellular survival (Lu et al., 2015) but induces autophagy and bacterial elimination (Nakagawa et al., 2004).

Rab41 is a Golgi-resident Rab GTPase that plays a role in anterograde trafficking of cargo from the ER to the Golgi and contributes to the maintenance of Golgi integrity (Haas et al., 2007). Rab41 was also previously referred to as Rab43, which is consistent with the human nomenclature. In the present study, we showed that Golgi-resident Rab41 is recruited to PcAV and that GTP binding to Rab41 is required for appropriate localization and efficient PcAV formation. We also show that PcAV formation is decreased in Rab41 KO MEFs with fragmented Golgi apparatus, reminiscent of the phenotype in cells treated with the Golgi disrupting agent BFA. Upon treatment with BFA, PcAV formation was also reduced, implying biological relevance of the biogenesis and maintenance of functional Golgi structures for PcAV formation. BFA also reportedly induces autophagy by inhibiting mTORC1 kinase activity on ribosomal S6 kinase (S6K) and is also used as a general inducer of autophagy (Desantis et al., 2015). Previously, GAS-induced autophagy was not influenced by BFA treatment (Oda et al., 2016), whereas noncanonical autophagy induced by sodium oleate was inhibited by BFA (Niso-Santano et al., 2015), indicating that noncanonical autophagy may be partially involved in the formation of PcAV.

Sodium oleate-induced noncanonical autophagy reportedly causes Golgi protein recruitment to autophagic puncta (Niso-Santano et al., 2015). In agreement, we showed that Rab41-positive PcAV were colocalized with GM130 expressing *cis*-Golgi and with Golgin-97 expressing *trans*-Golgi network (Figure 5c,d). However, the GFP-fused ER-Golgi intermediate compartment protein ERGIC53, which is a subunit of the conserved oligomeric Golgi complex COG6, and the ER-resident SNARE Sec22b were not colocalized with PcAV (Figure 5d). Thus, the relevance of Golgi apparatus and the origins of Rab41-positive PcAV membranes remain to be further investigated.

Previous study shows involvement of Rab41 in phagosomal maturation in *Mycobacterium tuberculosis*-infected macrophages (Seto, Tsujimura, & Koide, 2011). In our hand, LAMP-1 recruitment to PCV was not affected in Rab41 KO MEFs (Figure S5c). Moreover, previous studies show colocalization of Rab7, 9A, 17, 23, 30, and 35 with GAS-containing autophagic vesicles (GcAVs), and these Rabs are involved in GcAVs formation, GcAV-GcAV membrane fusion, and GcAVs maturation (Minowa-Nozawa, Nozawa, Okamoto-Furuta, Kohda, & Nakagawa, 2017; Nozawa et al., 2012; Yamaguchi et al., 2009). In our hands, Rab17, 23, 30, and 35 were not recruited to PcAV, indicating differing intracellular fates and autophagic responses of pyogenic-grouped GAS and mitis-grouped *S. pneumoniae*.

During selective autophagy of intracellular pathogens, bacteria were reportedly recognised by a variety of E3 ligases and were decorated with various types of poly-Ub chain (Galluzzi et al., 2017; Grumati & Dikic, 2017). K63Ub is the most favoured Ub type for autophagic recognition of intracellular pathogens (Grumati & Dikic, 2017). In the present study, K63Ub was deposited on PcAV following

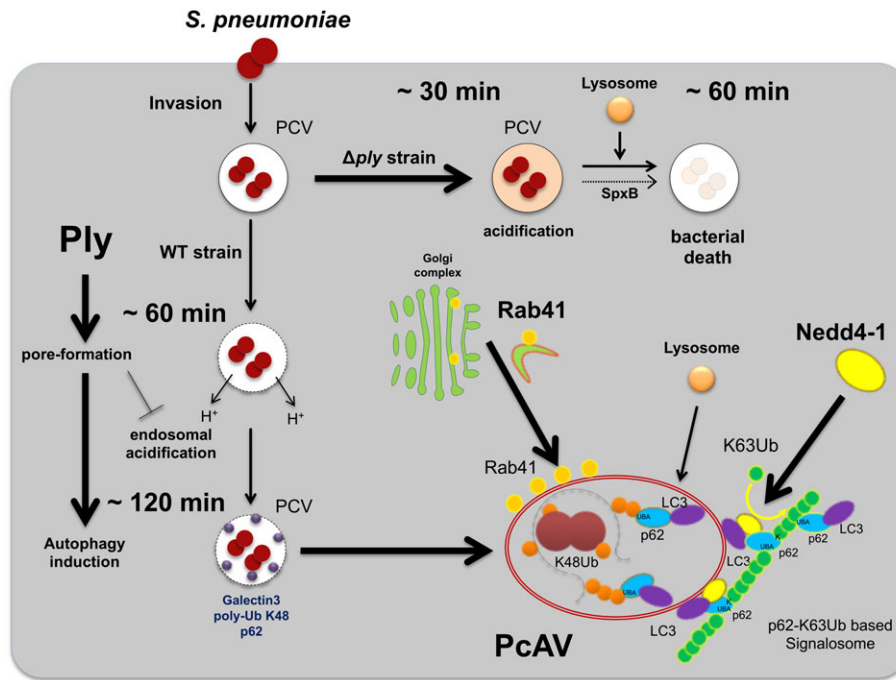


**FIGURE 7** Proposed model for intracellular fate of *Streptococcus pneumoniae* and K63Ub-linked signalosomes formation on *S. pneumoniae*-containing vesicles (PcAV). Ply provides advantages for bacteria to escape from endosomal elimination at early stages of infection. However, at late stage of infection, membrane remnants generated by Ply and cytosolic-exposed bacterial surface proteins are concomitant targets of selective autophagy via K48Ub-p62-LC3 autophagy cargo. Golgi-resident Rab41 is recruited to PcAV and involved in PcAV biogenesis. After PcAV formation, p62 and Nedd4-1 bind to LC3-II on autophagosome surfaces, and Nedd4-1 subsequently polyubiquitinates p62 through K63Ub. Generated K63Ub chains can cause cross-linking of LC3-p62 complexes on PcAV and may recruit other K63Ub-favouring cargo receptors on PcAV, leading to deposition of the K63Ub-mediated p62-signalosomes on PcAV

formation and numbers of K63Ub-positive PcAV-containing cells were not decreased during infection, suggesting that K63Ub is located outside of PcAV, or that K63Ub-bearing PcAV avoided autophagic maturation. In contrast, K48Ub was recruited to *S. pneumoniae* prior to the formation of PcAV in an Atg5-independent manner, and K48Ub was degraded over the time-course of infection by autophagy.

The HECT E3 ligases Nedd4-1 (Lin et al., 2017; Sun et al., 2017) and Nedd4-2 (Nedd4L) have also been associated with targeted autophagy (Lin et al., 2017; Sun et al., 2017), although Platta et al. reported that Nedd4-1 ubiquitinates Beclin-1 through K11 and is involved in the suppression of autophagy (Platta, Abrahamsen, Thoresen, & Stenmark, 2012). Therefore, we investigated the roles of Nedd4-1 in the regulation of selective autophagy in *S. pneumoniae*-infected cells using Nedd4-1-deficient MEFs and found that Nedd4-1 plays a pivotal role in K63Ub decoration and efficient formation of PcAV. Accordingly, we suggest that K63Ub is produced by LC3-Nedd4-1 interactions on PcAV surfaces and forms a scaffold for selective autophagy (p62-signalosome). Verlhac et al. also showed that LC3 on *Salmonella*-containing autophagosome surfaces can recruit NDP52, providing a foothold for autophagosome-endosome fusion (Verlhac et al., 2015). To test this hypothesis, we investigated whether Ub-p62-LC3 complexes enhance K63Ub and p62 recruitment to PcAV. Although p62 recruitment to *L. monocytogenes* in p62KO/ $\Delta$ LIR cells was fully recovered to levels observed in WT cells in our previous study (Yoshikawa et al., 2009), p62 recruitment to PCV was significantly decreased in p62KO/ $\Delta$ LIR cells in this study (Figure 3h). Hence, recruitment of Nedd4-1 by PcAV follows p62-

LC3 interactions and may lead to further p62 recruitment via K63Ub polyubiquitination of p62 (Figure 7). As shown in Figure 6d, K63Ub-positive PCV populations in p62 KO MEFs expressing  $\Delta$ UBA or  $\Delta$ LIR were reduced to about 50% of those in WT MEFs. Moreover, in Figure 3h, p62 recruitment to PCV and PcAV was also decreased in p62KO/K7A/D69A (PB1 domain-impaired mutant) MEFs. These results suggest that the PB1 domain is involved in oligomerisation of p62 and in enhancement of p62 and LC3 recruitment to PCV (or PcAV). These data are supported by a report showing that the PB1 domain is involved in binding of Nedd4-1 to p62 and that K7 of p62 is a major NEDD4 ubiquitination site (Lin et al., 2017).

The present discovery of novel interactions between *S. pneumoniae* and host cells gives new insights into the mechanisms, by which host defence systems sense *S. pneumoniae* and may facilitate the development of therapeutic targets for the control of pneumococcal infections and IPD.

## 4 | EXPERIMENTAL PROCEDURES

### 4.1 | Bacterial strains

*S. pneumoniae* strains R6 (ATCC BAA-255) and TIGR4 (ATCC BAA-334) were purchased from the American Type Culture Collection. *S. pneumoniae* were grown in standing cultures of Todd-Hewitt Broth (THY; BD) containing 0.5% yeast extract (BD) broth or were plated on THY agar plates or Columbia agar plates with 5% sheep blood (BD) at

37 °C in 5% CO<sub>2</sub>. *Escherichia coli* strains MC1061, DH10B, or C43 (Cosmo Bio) were used for DNA cloning and plasmid construction and were grown in LB broth or on LB agar plates supplemented with 100 µg/ml of ampicillin or 50 µg/ml of kanamycin. Detailed information about bacterial strains is shown in Table S1.

## 4.2 | Reagents and antibodies

Anti-Myc (9B11, Cell Signaling), anti-Flag (Wako), anti-multi-ubiquitin (FK2, MBL), anti-p62 (MBL), anti-K48 linked Ub (clone Apu2, EMD Millipore), anti-K63 linked Ub (clone Apu3, EMD Millipore), anti-M1 linked Ub (clone IE3, EMD Millipore), anti-LC3A/B (Cell Signaling), anti-Lamp1 (eBio), anti-GM130 (BD), anti-Ubc13 (Thermo Fisher Scientific), anti-*S. pneumoniae* (SSI), and anti-actin (Santa Cruz Biotechnology) were used as primary antibodies. HRP-conjugated goat anti-rabbit or anti-mouse antibodies (Jackson Laboratories) were used as secondary antibodies for immunoblotting. FITC-, TRITC- (Sigma-Aldrich), or Alexa647- (Thermo Fisher Scientific) conjugated goat anti-rabbit or anti-mouse IgG antibodies were used as secondary antibodies for immunostaining. DNA staining was performed using 4',6'-diamidino-2-phenylindole (DAPI; Sigma-Aldrich). Rapamycin (Selleck chemical), and PYR41 (UBPBio), 3-methyladenine (3-MA; Wako), bafilomycin A1 (Adipogen), BFA (Cayman Chemical), and E64d (Peptide Institute) were used as autophagy inducers or inhibitors. All other reagents were purchased from Sigma-Aldrich. LysoTracker DND-99 was purchased from Molecular Probes. Detailed information about antibodies and reagents is shown in Table S1.

## 4.3 | Plasmids

The vectors mCherry-LC3, p62-3Myc, ΔLIR, ΔUBA, ΔLIR/ΔUBA, K7AD69A, and p62-3Myc were constructed as described previously (Yoshikawa et al., 2009). GFP-Nedd4-1 and -Nedd4-2 expression vectors were constructed as previously described (Kawabe et al., 2010). pEGFP-C1 vectors (Clontech) carrying mouse Rab1-43 were prepared as described previously (Tsuboi & Fukuda, 2006). pEGFP-C1-Rab41(CA/CN) was also prepared as described previously (Ishida, Ohbayashi, Maruta, Ebata, & Fukuda, 2012). Rab15, Rab19, Rab38, Rab41, and Rab42 cDNA inserts in pEGFP-C1-Rab vectors were subcloned into the pmStrawberry-C1 vector (Ohbayashi, Maruta, Ishida, & Fukuda, 2012; Clontech). Murine Cog6 cDNA was amplified using PCR with the primers shown in Table S2 and pAct2-Cog6 as a template, and resulting DNA fragments were subcloned into the pEGFP-C1 vector (Fukuda, Kanno, Ishibashi, & Itoh, 2008). Human plgR, Vamp8, Vit1b, ERGIC53, Sec22b, LRSAM1, TRIM16, and Smurf1 cDNA were amplified using RT-PCR with SuperScript III One-Step RT-PCR System and Platinum Taq (Thermo Fisher Scientific) using the primer pairs shown in Table S2 and total mRNA from Detroit 562 or HeLa cell as a template. The resulting DNA fragments were subcloned into pEGFP-C (Clontech), pEGFP-N (Clontech), or pcDNA-3.1 (Invitrogen) vectors. Expression vectors for GFP-LC3 were a generous gift from Dr. Tamotsu Yoshimori (Osaka University; Kabeya et al., 2000). The expression vector encoding GFP-PARK2 was constructed by amplifying PARK2 from YFP-PARK2 using PCR (generous gift from Dr. Richard J. Youle [N. I. H.]) and cloning into pEGFP-C1 (Clontech).

The FLAG-Keap1 expression vector was a kind gift from Dr. Masaaki Komatsu (Ichimura et al., 2013). Detailed information about plasmids is shown in Table S1.

## 4.4 | Recombinant retroviruses and retroviral infections

The pMXs-puro and pMX-IRES-blast vectors were purchased from Cosmo Bio. To generate recombinant retroviruses, cDNAs corresponding to plgR and GFP-LC3 were cloned into pMXs-puro and pMX-IRES-blast vectors. Subsequently, mCherry-LC3 or p62-3Myc (FL, ΔLIR, ΔUBA, ΔLIR/ΔUBA, or K7AD69A) were cloned into pMXs-puro. GFP-Galectin3, Rab41 (WT, CA, and CN), Nedd4-1, and Nedd4-2 were cloned into pMX-IRES-blast vectors. Recombinant retroviruses were prepared as previously described (Yoshikawa et al., 2009). Briefly, retroviral plasmids were transfected into Plat-E, and after 2-day culture, supernatants containing retrovirus were collected and centrifugated, and clear supernatants were used for retroviral infections. After introduction of retrovirus into non-mouse cells, such as BHK and Detroit 562 cells, constructed retroviral vectors were transfected into Plat-E cells with a VSV-G envelope expressing vector. Recipient cells were infected with retroviruses by adding supernatants from Plat-E cells in the presence of polybrene for 6 hr. Stable transformants were selected in Dulbecco's modified Eagle's medium (DMEM) containing 10% fetal calf serum (FCS) and 1 µg/ml of puromycin or 10 µg/ml of blasticidin.

## 4.5 | Cell culture and transfection

BHK, Detroit 562 human pharynx epithelial, 293T human embryonic kidney cells, WT MEFs, p62 KO MEFs, TRAF6 KO MEFs, Rab41 KO MEFs, Nedd4-1 KO (Kawabe et al., 2010; Kobayashi et al., 2001; Komatsu et al., 2007), and autophagy-deficient MEFs (Atg5 KO, Atg7 KO, Atg16L1 KO (Δ/Δ), FIP200 KO, and ULK1/2 double KO cells; Cheong, Lindsten, Wu, Lu, & Thompson, 2011; Hara et al., 2008; Komatsu et al., 2005; Kuma et al., 2004; Saitoh et al., 2008) were cultured in DMEM (Nakarai) supplemented with 10% FCS, 100 µg/ml of gentamicin (Wako), and 60 µg/ml of kanamycin (Wako). Ubc13<sup>fllox/fllox</sup>/CRE MEFs were cultured in DMEM supplemented with 10% FCS and 1 µg/ml of puromycin (Sigma-Aldrich; Yamamoto et al., 2006), and Plat-E cells were maintained in DMEM containing 10% FCS, 10 µg/ml of puromycin, and 10 µg/ml of blasticidin (Kaken Pharmaceutical). BHK cells stably expressing EGFP-LC3 or mCherry-LC3 were maintained in DMEM containing 10% FCS and 1,000 µg/ml of G418 (Roche). Transfections were performed using PEI MAX (Polysciences) for 293T cells, Lipofectamine LTX (Invitrogen) for Plat-E cells, and Fugene 6 (Promega) for BHK cells and MEFs according to the manufacturer's protocols. Detailed information about cell lines is shown in Table S1.

## 4.6 | Construction of *S. pneumoniae* mutant strains

Inactivation of the *ply* gene in *S. pneumoniae* strain R6 was performed by double cross-over recombination as described previously. Briefly, an *erm* cassette with long flanking regions that are homologous to the target gene were generated using two-step PCR as described

previously (Yamamoto, Izumiya, Morita, Arakawa, & Watanabe, 2009) using the primers listed in Table S3. PCR products were used to transform competent cells of the *S. pneumoniae* strain R6. To prepare competent cells, bacteria were grown in THY broth to OD<sub>600</sub> = 0.25, and cultures were frozen in 15% glycerol at -80 °C. Prior to transformation, 50 µl of frozen cell samples were thawed and diluted in 1 ml of aliquots of prewarmed competence medium (Tryptic soy broth [pH 8.0], 10% glycerol, 0.16% bovine serum albumin, 0.01% CaCl<sub>2</sub>) containing 200 ng of CSP-1 (Anaspec) and 1 µg of transforming DNA (Pozzi et al., 1996). Transformation reactions were performed for 180 min at 37 °C under aerobic conditions with constant agitation, and small aliquots were plated on THY agar plates supplemented 1 µg/ml of erythromycin and were incubated for 24 hr at 37 °C. Inactivation of the *ply* gene was confirmed using PCR with the primers shown in Table S3. The *ply/spxB* double KO mutant was generated using the same procedures with the *ply* mutant as a parental strain, and transformants were selected using 2 µg/ml of erythromycin. Inactivation of *ply* and *spxB* genes was confirmed using PCR with the primers shown in Table S3.

#### 4.7 | Infection with *S. pneumoniae* and visualisation of PcAV

BHK, MEF, and Detroit 562 cells were seeded at  $2 \times 10^5$  cells per well on glass coverslips in 6-well plates. To prepare frozen starting culture stocks, *S. pneumoniae* were grown in THY broth to OD<sub>600</sub> = 0.3, and cultures were chilled on ice for 10 min, mixed with ice-cold 50% glycerol at a ratio of 2:1, and were stored frozen in 200 µl of aliquots at -80 °C. Prior to infection experiments, 200 µl of aliquots of frozen bacterial cells were thawed and diluted in 5 ml of aliquots of prewarmed THY medium and were then grown to OD = 0.25 as standing cultures at 37 °C in 5% CO<sub>2</sub>. The resulting bacterial suspensions were diluted in bacterial suspension buffer comprising MEM supplemented with 1% FCS, 25-mM HEPES (pH 7.8), and 6.7 µg/ml of catalase (Sigma-Aldrich). Suspensions were then added to wells at a multiplicity of infection of 100 and were then centrifuged at 1,000 rpm for 5 min at room temperature. Cells were then incubated for 1 hr at 37 °C in 5% CO<sub>2</sub>, were washed with Hank's balanced salt solution (HBSS) 3 times, and were then incubated for 30 min in DMEM/10% FCS containing 200 µg/ml of gentamicin and 6.7 µg/ml of catalase to eliminate extracellular bacteria. Culture media were then replaced with DMEM containing 10% FCS with 100 µg/ml of gentamicin and 6.7 µg/ml of catalase (incubation buffer), and cells were incubated for the indicated periods at 37 °C in 5% CO<sub>2</sub>. If not stated otherwise, inhibitors were added in incubation buffer to avoid influences on bacterial invasion efficiency. At each time point, cells were fixed with 4% paraformaldehyde in phosphate-buffered saline (PBS; Wako) for 15 min at room temperature. Fixed cells were then washed with PBS 3 times, were quenched with 50-mM NH<sub>4</sub>Cl in PBS for 10 min, were permeabilised with 0.2% Triton X-100 in PBS for 10 min, and were finally blocked with 2% bovine serum albumin in Tris-buffered saline for 30 min at room temperature. After staining with indicated antibodies, specimens were analysed using confocal microscopy (Carl Zeiss LSM700). For Western blot analyses, cells were washed with PBS 3 times and were directly lysed with 100 µl of

2 × SDS sample buffer (Nakarai Tesque) per well. Equal volumes of lysates were separated using SDS-PAGE and were then transferred to polyvinylidene difluoride membranes. For electron microscopy observations, cells were seeded on 35-mm dishes, were infected with *S. pneumoniae* as described above, were fixed with 2% glutaraldehyde/4% paraformaldehyde in PBS overnight at room temperature, were post fixed in 2% OsO<sub>4</sub>, were dehydrated with a graded ethanol series, and were finally embedded in epoxy resin. Ultrathin sections were stained with uranyl acetate and lead citrate.

#### 4.8 | Quantification of cells containing bacteria-associated autophagic markers

Numbers of cells with PCV associated with autophagic markers, such as GFP-LC3, p62-3Myc, and ubiquitin, were determined by visual counting using fluorescence microscopy. At least 500 PCV, PcAV, or pneumococcus-containing cells were examined in triplicate for each experimental condition. Error bars indicate standard errors of the mean.

#### 4.9 | Intracellular bacterial survivability assays

MEFs were seeded on 24-well plates and were infected with WT or *ply* strains of *S. pneumoniae* as described above. After centrifugation, cells were incubated for 1 hr at 37 °C in 5% CO<sub>2</sub>, were washed with HBSS twice, and were then incubated in 500 µl of aliquots of DMEM/10% FCS with 200 µg/ml of gentamicin and 6.7 µg/ml of catalase for 15 min. Extracellular bacteria were eradicated by incubating in DMEM containing 10% FCS, 200 µg/ml of gentamicin, 6.7 µg/ml of catalase, and 20 µg/ml of penicillin G (Wako) for a further 15 min. After washing cells with HBSS 3 times, cells were incubated in DMEM containing 10% FCS and 6.7 µg/ml of catalase for indicated periods at 37 °C in 5% CO<sub>2</sub> and were then lysed using 1.0% saponin (Sigma-Aldrich) in PBS. Lysates were serially diluted with 0.1% saponin in PBS and were plated onto THY-agar plates, and numbers of intracellular bacteria were finally counted and expressed in colony forming units (cfu).

#### 4.10 | siRNA

siRNAs were synthesised and duplexed by Nippon Gene. The siRNA sequences for mouse Rabs are shown in Table S4. Universal negative control siRNA was purchased from Nippon Gene. siRNAs were transfected into cells using reverse transfection with Lipofectamine RNAi MAX (Invitrogen) according to the manufacturer's protocol. Rab41 expression levels were then confirmed using by RT-PCR with the primer pairs listed in Table S3. RNA from MEFs was extracted using RNeasy Mini Kits (QIAGEN).

#### 4.11 | Synthesis of CRISPR plasmids

To perform genome editing using puromycin as a selection marker, pSELECT-CRISPR-CAS9 plasmids were constructed as follows: Initially, pSELECT-puro-L1 plasmid was modified by removal of the hEF1α-HTLV promoter and disruption of the BsmBI restriction site, and PCR fragments of U6-sgRNA-EFS-SpCAS9 from lentiCRISPR

were inserted into the plasmids (Yamaji & Hanada, 2014). Plasmids were then cleaved with *Bsm*BI, and 20-mer guide sequences were ligated into the site. The guide sequences are listed in Table S5.

#### 4.12 | Construction of CRISPR KO cell lines

On Day 0, MEFs ( $2.0 \times 10^5$  cells per well in 6-well plates) were cultured overnight and on Day 1 were transfected with a CRISPR plasmid using lipofectamine 3000 (Thermo Fisher Scientific) according to the manufacturer's protocols. On Day 2, cells were transferred to 10-cm dishes and were cultured at 37 °C with puromycin at 5 µg/ml, which is higher than the usual concentration and was used to concentrate cells with higher expression of sgRNAs. On Day 4, the culture medium was replaced with puromycin-free medium, and cells were subcultured for 1 week. CRISPR-treated MEFs were then harvested for indel analyses or were diluted to isolate gene-disrupted clones. Indel analyses were performed as previously described (Yamaji & Hanada, 2014). Briefly, trypsinised cells were simply heated in TE buffer followed by vortexing for use as genomic DNA templates for PCR. PCR was performed using AmpliTaq360 DNA polymerase, and DNA sequences of PCR products were analysed using the primer pairs shown in Table S5. After indel analyses, CRISPR-treated MEFs were diluted to isolate gene-disrupted clones. Gene disruption was confirmed using PCR with genomic DNA template and the primer pairs shown in Table S5. DNA fragments were then subcloned into pBluescript SKII (+; Stratagene) vectors, and DNA sequences were analysed.

#### 4.13 | Quantification and statistical analysis

At least 500 PCV, PcAV, or pneumococcus-containing cells were examined in triplicate for each experiment. Data are expressed as means  $\pm$  SEM. *p* values were calculated using Student's *t* test, and when standard deviations were significantly different ( $F < 0.05$ ), experimental differences were identified using Mann–Whitney *U* test. All statistical analyses were performed using Prism6.

#### ACKNOWLEDGEMENTS

We thank Drs. Tamotsu Yoshimori, Tatsuya Saitoh, Shizuo Akira, Craig B. Thompson, Masaaki Komatsu, and Noboru Mizushima for providing reagents. This work was supported by Grant-in-Aid for Scientific Research on Innovative Areas (16H01189 and 17H05682) to M. F. and by Grant-in-Aid for Scientific Research (C) (16K08800 and 25460555) to Mi. O. from the Ministry of Education, Culture, Sports, Science, and Technology (MEXT). This work was supported by grants from the Naito Foundation and the Uehara Memorial Foundation. The authors have no conflicting financial interests.

#### ORCID

Michinaga Ogawa  <http://orcid.org/0000-0001-6883-6443>

Mitsunori Fukuda  <http://orcid.org/0000-0002-8620-5853>

#### REFERENCES

- Barnett, T. C., Cole, J. N., Rivera-Hernandez, T., Henningham, A., Paton, J. C., Nizet, V., & Walker, M. J. (2015). Streptococcal toxins: Role in pathogenesis and disease. *Cellular Microbiology*, 17, 1721–1741.
- Beauregard, K. E., Lee, K. D., Collier, R. J., & Swanson, J. A. (1997). pH-dependent perforation of macrophage phagosomes by listeriolysin O from *Listeria monocytogenes*. *The Journal of Experimental Medicine*, 186, 1159–1163.
- Chao, Y., Marks, L. R., Pettigrew, M. M., & Hakansson, A. P. (2014). Streptococcus pneumoniae biofilm formation and dispersion during colonization and disease. *Frontiers in Cellular and Infection Microbiology*, 4, 194.
- Cheong, H., Lindsten, T., Wu, J., Lu, C., & Thompson, C. B. (2011). Ammonia-induced autophagy is independent of ULK1/ULK2 kinases. *Proceedings of the National Academy of Sciences of the United States of America*, 108, 11121–11126.
- Desantis, A., Bruno, T., Catena, V., De Nicola, F., Goeman, F., Iezzi, S., et al. (2015). Che-1-induced inhibition of mTOR pathway enables stress-induced autophagy. *The EMBO Journal*, 34, 1214–1230.
- Echlin, H., Frank, M. W., Iverson, A., Chang, T. C., Johnson, M. D., Rock, C. O., & Rosch, J. W. (2016). Pyruvate oxidase as a critical link between metabolism and capsule biosynthesis in *Streptococcus pneumoniae*. *PLoS Pathogens*, 12, e1005951.
- Fujita, N., Morita, E., Itoh, T., Tanaka, A., Nakaoka, M., Osada, Y., ... Yoshimori, T. (2013). Recruitment of the autophagic machinery to endosomes during infection is mediated by ubiquitin. *The Journal of Cell Biology*, 203, 115–128.
- Fukuda, M., Kanno, E., Ishibashi, K., & Itoh, T. (2008). Large scale screening for novel rab effectors reveals unexpected broad Rab binding specificity. *Molecular & Cellular Proteomics*, 7, 1031–1042.
- Furuta, N., Fujita, N., Noda, T., Yoshimori, T., & Amano, A. (2010). Combinational soluble N-ethylmaleimide-sensitive factor attachment protein receptor proteins VAMP8 and Vti1b mediate fusion of antimicrobial and canonical autophagosomes with lysosomes. *Molecular Biology of the Cell*, 21, 1001–1010.
- Galluzzi, L., Baehrecke, E. H., Ballabio, A., Boya, P., Bravo-San Pedro, J. M., Cecconi, F., ... Kroemer, G. (2017). Molecular definitions of autophagy and related processes. *The EMBO Journal*, 36, 1811–1836.
- Gradstedt, H., Iovino, F., & Bijlsma, J. J. (2013). Streptococcus pneumoniae invades endothelial host cells via multiple pathways and is killed in a lysosome dependent manner. *PLoS one*, 8, e65626.
- Grumati, P., & Dikic, I. (2017). Ubiquitin signaling and autophagy. *The Journal of Biological Chemistry*, jbc.TM117.000117.
- Haas, A. K., Yoshimura, S., Stephens, D. J., Preisinger, C., Fuchs, E., & Barr, F. A. (2007). Analysis of GTPase-activating proteins: Rab1 and Rab43 are key Rabs required to maintain a functional Golgi complex in human cells. *Journal of Cell Science*, 120, 2997–3010.
- Haldar, A. K., Foltz, C., Finethy, R., Piro, A. S., Feeley, E. M., Pilla-Moffett, D. M., ... Coers, J. (2015). Ubiquitin systems mark pathogen-containing vacuoles as targets for host defense by guanylate binding proteins. *Proceedings of the National Academy of Sciences of the United States of America*, 112, E5628–E5637.
- Hara, T., Takamura, A., Kishi, C., Iemura, S., Natsume, T., Guan, J. L., & Mizushima, N. (2008). FIP200, a ULK-interacting protein, is required for autophagosome formation in mammalian cells. *The Journal of Cell Biology*, 181, 497–510.
- Henry, R., Shaughnessy, L., Loessner, M. J., Alberti-Segui, C., Higgins, D. E., & Swanson, J. A. (2006). Cytolysin-dependent delay of vacuole maturation in macrophages infected with *Listeria monocytogenes*. *Cellular Microbiology*, 8, 107–119.
- Ichimura, Y., Waguri, S., Sou, Y. S., Kageyama, S., Hasegawa, J., Ishimura, R., ... Komatsu, M. (2013). Phosphorylation of p62 activates the Keap1-Nrf2 pathway during selective autophagy. *Molecular Cell*, 51, 618–631.
- Ishida, M., Ohbayashi, N., Maruta, Y., Ebata, Y., & Fukuda, M. (2012). Functional involvement of Rab1A in microtubule-dependent anterograde melanosome transport in melanocytes. *Journal of Cell Science*, 125, 5177–5187.
- Kabaya, Y., Mizushima, N., Ueno, T., Yamamoto, A., Kirisako, T., Noda, T., ... Yoshimori, T. (2000). LC3, a mammalian homologue of yeast Apg8p, is

- localized in autophagosome membranes after processing. *The EMBO Journal*, 19, 5720–5728.
- Kadioglu, A., Weiser, J. N., Paton, J. C., & Andrew, P. W. (2008). The role of *Streptococcus pneumoniae* virulence factors in host respiratory colonization and disease. *Nature Reviews. Microbiology*, 6, 288–301.
- Kawabe, H., Neeb, A., Dimova, K., Young, S. M. Jr., Takeda, M., Katsurabayashi, S., et al. (2010). Regulation of Rap2A by the ubiquitin ligase Nedd4-1 controls neurite development. *Neuron*, 65, 358–372.
- Kim, J. Y., Paton, J. C., Briles, D. E., Rhee, D. K., & Pyo, S. (2015). *Streptococcus pneumoniae* induces pyroptosis through the regulation of autophagy in murine microglia. *Oncotarget*, 6, 44161–44178.
- Kobayashi, N., Kadono, Y., Naito, A., Matsumoto, K., Yamamoto, T., Tanaka, S., & Inoue, J. (2001). Segregation of TRAF6-mediated signaling pathways clarifies its role in osteoclastogenesis. *The EMBO Journal*, 20, 1271–1280.
- Komatsu, M., Waguri, S., Koike, M., Sou, Y. S., Ueno, T., Hara, T., ... Tanaka, K. (2007). Homeostatic levels of p62 control cytoplasmic inclusion body formation in autophagy-deficient mice. *Cell*, 131, 1149–1163.
- Komatsu, M., Waguri, S., Ueno, T., Iwata, J., Murata, S., Tanida, I., ... Chiba, T. (2005). Impairment of starvation-induced and constitutive autophagy in Atg7-deficient mice. *The Journal of Cell Biology*, 169, 425–434.
- Kuma, A., Hatano, M., Matsui, M., Yamamoto, A., Nakaya, H., Yoshimori, T., ... Mizushima, N. (2004). The role of autophagy during the early neonatal starvation period. *Nature*, 432, 1032–1036.
- Li, P., Shi, J., He, Q., Hu, Q., Wang, Y. Y., Zhang, L. J., et al. (2015). *Streptococcus pneumoniae* induces autophagy through the inhibition of the PI3K-I/Akt/mTOR pathway and ROS hypergeneration in A549 cells. *PLoS one*, 10, e0122753
- Lin, Q., Dai, Q., Meng, H., Sun, A., Wei, J., Peng, K., ... Yang, W. (2017). The HECT E3 ubiquitin ligase NEDD4 interacts with and ubiquitinates SQSTM1 for inclusion body autophagy. *Journal of Cell Science*, 130, 3839–3850.
- Lu, S. L., Kuo, C. F., Chen, H. W., Yang, Y. S., Liu, C. C., Anderson, R., et al. (2015). Insufficient acidification of autophagosomes facilitates Group A streptococcus survival and growth in endothelial cells. *MBio*, 6, e01435–e01415.
- Minowa-Nozawa, A., Nozawa, T., Okamoto-Furuta, K., Kohda, H., & Nakagawa, I. (2017). Rab35 GTPase recruits NPD52 to autophagy targets. *The EMBO Journal*, 36, 2790–2807.
- Nakagawa, I., Amano, A., Mizushima, N., Yamamoto, A., Yamaguchi, H., Kamimoto, T., ... Yoshimori, T. (2004). Autophagy defends cells against invading Group A streptococcus. *Science*, 306, 1037–1040.
- Nakano, S., Fujisawa, T., Ito, Y., Chang, B., Suga, S., Noguchi, T., ... Ichiyama, S. (2016). Serotypes, antimicrobial susceptibility, and molecular epidemiology of invasive and non-invasive *Streptococcus pneumoniae* isolates in paediatric patients after the introduction of 13-valent conjugate vaccine in a nationwide surveillance study conducted in Japan in 2012–2014. *Vaccine*, 34, 67–76.
- Niso-Santano, M., Malik, S. A., Pietrocola, F., Bravo-San Pedro, J. M., Marino, G., Cianfanelli, V., ... Kroemer, G. (2015). Unsaturated fatty acids induce non-canonical autophagy. *The EMBO Journal*, 34, 1025–1041.
- Nozawa, T., Aikawa, C., Goda, A., Maruyama, F., Hamada, S., & Nakagawa, I. (2012). The small GTPases Rab9A and Rab23 function at distinct steps in autophagy during Group A streptococcus infection. *Cellular Microbiology*, 14, 1149–1165.
- Oda, S., Nozawa, T., Nozawa-Minowa, A., Tanaka, M., Aikawa, C., Harada, H., & Nakagawa, I. (2016). Golgi-resident GTPase Rab30 promotes the biogenesis of pathogen-containing autophagosomes. *PLoS one*, 11, e0147061
- Ogawa, M., Yoshikawa, Y., Kobayashi, T., Mimuro, H., Fukumatsu, M., Kiga, K., ... Sasakawa, C. (2011). A Tecpr1-dependent selective autophagy pathway targets bacterial pathogens. *Cell Host & Microbe*, 9, 376–389.
- Ogawa, M., Yoshimori, T., Suzuki, T., Sagara, H., Mizushima, N., & Sasakawa, C. (2005). Escape of intracellular *Shigella* from autophagy. *Science*, 307, 727–731.
- Ohbayashi, N., Maruta, Y., Ishida, M., & Fukuda, M. (2012). Melanoregulin regulates retrograde melanosome transport through interaction with the RILP-p150Glued complex in melanocytes. *Journal of Cell Science*, 125, 1508–1518.
- Platta, H. W., Abrahamson, H., Thoresen, S. B., & Stenmark, H. (2012). Nedd4-dependent lysine-11-linked polyubiquitination of the tumour suppressor Beclin 1. *The Biochemical Journal*, 441, 399–406.
- Pozzi, G., Masala, L., Iannelli, F., Manganelli, R., Havarstein, L. S., Piccoli, L., ... Morrison, D. A. (1996). Competence for genetic transformation in encapsulated strains of *Streptococcus pneumoniae*: Two allelic variants of the peptide pheromone. *Journal of Bacteriology*, 178, 6087–6090.
- Regev-Yochay, G., Trzcinski, K., Thompson, C. M., Lipsitch, M., & Malley, R. (2007). SpxB is a suicide gene of *Streptococcus pneumoniae* and confers a selective advantage in an in vivo competitive colonization model. *Journal of Bacteriology*, 189, 6532–6539.
- Saitoh, T., Fujita, N., Jang, M. H., Uematsu, S., Yang, B. G., Satoh, T., ... Akira, S. (2008). Loss of the autophagy protein Atg16L1 enhances endotoxin-induced IL-1beta production. *Nature*, 456, 264–268.
- Seto, S., Tsujimura, K., & Koide, Y. (2011). Rab GTPases regulating phagosome maturation are differentially recruited to mycobacterial phagosomes. *Traffic*, 12, 407–420.
- Sun, A., Wei, J., Childress, C., Shaw, J. H.t., Peng, K., Shao, G., et al. (2017). The E3 ubiquitin ligase NEDD4 is an LC3-interactive protein and regulates autophagy. *Autophagy*, 13, 522–537.
- Tsui, T., & Fukuda, M. (2006). Rab3A and Rab27A cooperatively regulate the docking step of dense-core vesicle exocytosis in PC12 cells. *Journal of Cell Science*, 119, 2196–2203.
- Verlhac, P., Gregoire, I. P., Azocar, O., Petkova, D. S., Baguet, J., Viret, C., & Faure, M. (2015). Autophagy receptor NDP52 regulates pathogen-containing autophagosome maturation. *Cell Host & Microbe*, 17, 515–525.
- Yamaguchi, H., Nakagawa, I., Yamamoto, A., Amano, A., Noda, T., & Yoshimori, T. (2009). An initial step of GAS-containing autophagosome-like vacuoles formation requires Rab7. *PLoS Pathogens*, 5, e1000670
- Yamaji, T., & Hanada, K. (2014). Establishment of HeLa cell mutants deficient in sphingolipid-related genes using TALENs. *PLoS one*, 9, e88124
- Yamamoto, M., Okamoto, T., Takeda, K., Sato, S., Sanjo, H., Uematsu, S., ... Akira, S. (2006). Key function for the Ubc13 E2 ubiquitin-conjugating enzyme in immune receptor signaling. *Nature Immunology*, 7, 962–970.
- Yamamoto, S., Izumiya, H., Morita, M., Arakawa, E., & Watanabe, H. (2009). Application of lambda Red recombination system to *Vibrio cholerae* genetics: Simple methods for inactivation and modification of chromosomal genes. *Gene*, 438, 57–64.
- Yoshikawa, Y., Ogawa, M., Hain, T., Yoshida, M., Fukumatsu, M., Kim, M., ... Sasakawa, C. (2009). *Listeria monocytogenes* ActA-mediated escape from autophagic recognition. *Nature Cell Biology*, 11, 1233–1240.
- Zhang, J. R., Mostov, K. E., Lamm, M. E., Nanno, M., Shimida, S., Ohwaki, M., & Tuomanen, E. (2000). The polymeric immunoglobulin receptor translocates pneumococci across human nasopharyngeal epithelial cells. *Cell*, 102, 827–837.

## SUPPORTING INFORMATION

Additional Supporting Information may be found online in the supporting information tab for this article.

**How to cite this article:** Ogawa M, Matsuda R, Takada N, et al. Molecular mechanisms of *Streptococcus pneumoniae*-targeted autophagy via pneumolysin, Golgi-resident Rab41, and Nedd4-1-mediated K63-linked ubiquitination. *Cellular Microbiology*. 2018;20:e12846. <https://doi.org/10.1111/cmi.12846>